EARTH SURFACE PROCESSES AND LANDFORMS
Earth Surf. Process. Landforms **44**, 918–932 (2019)

Published online 2 December 2018 in Wiley Online Library
(wileyonlinelibrary.com) DOI: 10.1002/esp.4544

Ice cap erosion patterns from bedrock ^{10}Be and ^{26}Al, southeastern Tibetan Plateau

Ping Fu,[1]* Arjen P. Stroeven,[2] Jonathan M. Harbor,[2,3] Jakob Heyman,[4] Clas Hättestrand[2] and Marc W. Caffee[3,5]

[1] School of Geographical Sciences, University of Nottingham Ningbo China, 199 Taikang East Road, Ningbo, 315100 Zhejiang, P.R. China

[2] Geomorphology & Glaciology, Department of Physical Geography, Stockholm University, Stockholm, Sweden and Bolin Centre for Climate Research, Stockholm University, Stockholm, Sweden

[3] Department of Earth, Atmospheric, and Planetary Sciences, Purdue University, West Lafayette, USA

[4] Department of Earth Sciences, University of Gothenburg, Gothenburg, Sweden

[5] Department of Physics and Astronomy, Purdue University, West Lafayette, USA

Received 7 September 2017; Revised 29 October 2018; Accepted 1 November 2018

*Correspondence to: Ping Fu, School of Geographical Sciences, University of Nottingham Ningbo China, 199 Taikang East Road, Ningbo, 315100 Zhejiang, P.R. China. E-mail: ping.fu@nottingham.edu.cn

Earth Surface Processes and Landforms

ABSTRACT: Quantifying glacial erosion contributes to our understanding of landscape evolution and topographic relief production in high altitude and high latitude areas. Combining *in situ* ^{10}Be and ^{26}Al analysis of bedrock, boulder, and river sand samples, geomorphological mapping, and field investigations, we examine glacial erosion patterns of former ice caps in the Shaluli Shan of the southeastern Tibetan Plateau. The general landform pattern shows a zonal pattern of landscape modification produced by ice caps of up to 4000 km^2 during pre-LGM (Last Glacial Maximum) glaciations, while the dating results and landforms on the plateau surface imply that the LGM ice cap further modified the scoured terrain into different zones. Modeled glacial erosion depth of 0–0.38 m per 100 ka bedrock sample located close to the western margin of the LGM ice cap, indicates limited erosion prior to LGM and Late Glacial moraine deposition. A strong erosion zone exists proximal to the LGM ice cap marginal zone, indicated by modeled glacial erosion depth >2.23 m per 100 ka from bedrock samples. Modeled glacial erosion depths of 0–1.77 m per 100 ka from samples collected along the edge of a central upland, confirm the presence of a zone of intermediate erosion in-between the central upland and the strong erosion zone. Significant nuclide inheritance in river sand samples from basins on the scoured plateau surface also indicate restricted glacial erosion during the last glaciation. Our study, for the first time, shows clear evidence for preservation of glacial landforms formed during previous glaciations under non-erosive ice on the Tibetan Plateau. As patterns of glacial erosion intensity are largely driven by the basal thermal regime, our results confirm earlier inferences from geomorphology for a concentric basal thermal pattern for the Haizishan ice cap during the LGM. © 2018 John Wiley & Sons, Ltd.

KEYWORDS: glacial erosion pattern; Tibetan Plateau; basal thermal regime; Last Glacial Maximum; ^{10}Be

Introduction

Erosion by glaciers and ice sheets over multiple glacial cycles is responsible for producing diverse landscapes, generating and reducing relief, perturbing geochemical processes, and thereby contributing to climate oscillations during the Quaternary Period (Montgomery, 2002; Brook *et al.*, 2006; Koppes and Montgomery, 2009; Brocklehurst, 2010; Jaeger and Koppes, 2016; Egholm *et al.*, 2017; Torres *et al.*, 2017). Erosion plays a dominant role in landscape evolution, so placing constraints on glacial erosion depths and patterns will enable a better understanding of the relative importance of the different drivers of these erosional processes (Hallet *et al.*, 1996; Koppes *et al.*, 2015; Herman *et al.*, 2018). The patterns and depths of erosion by ice sheets and alpine glaciers have been investigated using diverse methodologies, including: measurements of sediment yields (Hallet *et al.*, 1996; Hooke and Elverhøi, 1996; Koppes and Hallet, 2006; Delmas *et al.*, 2009; Dowdeswell *et al.*, 2010; Cowan *et al.*, 2010), reconstruction of pre-glacial topographic features (Andrews and LeMasurier, 1973; Nesje *et al.*, 1992; Montgomery, 2002; Amundson and Iverson, 2006; Brook *et al.*, 2008; van der Beek and Bourbon, 2008; Swift *et al.*, 2008), and through numerical modeling (Harbor *et al.*, 1988; Harbor, 1992, 1995; MacGregor *et al.*, 2000, 2009). These methods typically provide spatially averaged erosion rates or focus on valley cross- and long-section evolution, undermining their ability to constrain erosion patterns in finer detail. Aiming to understand large-scale landscape evolution, 2-D and 3-D numerical models of glacial landscape evolution have been employed for alpine glaciers (Braun *et al.*, 1999; Tomkin and Braun, 2002; Brocklehurst and Whipple, 2006; Herman and Braun, 2008; Egholm *et al.*, 2012; Yanites and Ehlers, 2012; Sternai *et al.*, 2013) and continental ice sheets (Jamieson *et al.*, 2008, 2010; Kleman *et al.*, 2008; Melanson *et al.*, 2013; Ugelvig *et al.*, 2016; Patton *et al.*, 2017). The modeling approaches are powerful for studying large-scale landscape evolution, but they remain simplified representations of natural systems. Field observations are needed to make these models more accurate indicators of real-world geologic processes.

In recent decades, our ability to reconstruct both the timing of glaciations, and in some cases patterns of erosion, has improved with the development and application of *in situ* cosmogenic nuclides techniques (cf. Gosse and Phillips, 2001; Balco, 2011; Heyman *et al*., 2011b; Granger *et al*., 2013). Quantifying glacial erosion using these techniques is based on the recognition that inheritance of cosmogenic nuclides from prior exposure indicates incomplete erosional resetting (Briner and Swanson, 1998; Davis *et al*., 1999; Fabel and Harbor, 1999; Colgan *et al*., 2002; Fabel *et al*., 2002, 2004; Stroeven *et al*., 2002a, b; Briner *et al*., 2003, 2014; Marquette *et al*., 2004; Li *et al*., 2005; Harbor *et al*., 2006; Miller *et al*., 2006; Staiger *et al*., 2006; Ivy-Ochs *et al*., 2014; Knudsen and Egholm, 2018). With two nuclides of different half-lives, such as ^{10}Be and ^{26}Al, it is also possible to reconstruct the burial and exposure history of bedrock samples, and thus infer basal thermal regimes over periods of more than hundreds of thousands of years (Bierman *et al*., 1999; Stroeven *et al*., 2002b; Staiger *et al*., 2005; Phillips *et al*., 2006; Li *et al*., 2008; Knudsen *et al*., 2015; Sugden *et al*., 2017). Low erosion rates would allow for inferring basal regimes across several hundreds of thousands of years.

Previous studies of glacial erosion on the Tibetan Plateau have included geomorphological mapping, sedimentological analyses, numerical glacial and climate modeling, and cosmogenic dating studies (Cui, 1981a, b; Zheng and Ma, 1995; Li *et al*., 2001; Schäfer *et al*., 2002; Owen *et al*., 2003, 2005, 2006; Graf *et al*., 2008; Rahaman *et al*., 2009; Seong *et al*., 2009a, b; Stroeven *et al*., 2009; Whipple, 2009; Heyman *et al*., 2011a, b). These studies have focused primarily on alpine valley glacial systems. The Shaluli Shan, located in the southeastern Tibetan Plateau, offers a different glacial setting in which local ice caps and outlet glaciers co-existed with valley glaciers during glacial cycles (Li *et al*., 1991; Shi, 1992, 2002; Fu *et al*., 2012, 2013a, b; Figure 1).

Landforms on the Haizishan Plateau in the Shaluli Shan show evidence for a rich history of ice cap glaciation (Fu *et al*., 2013a). These landforms display a distribution of erosion and deposition similar to those produced by continental-scale ice sheets (Sugden, 1978; Kleman *et al*., 2008). Four characteristic and concentric landform zones have been identified (Zheng and Ma, 1995; Fu *et al*., 2013a; Figure 2(B)). The outermost, Zone I in Figure 2(B), consists of glacial deposits and includes large marginal moraines located beyond the mouths of outlet valleys. Zone II, set within Zone 1, consists of deeply incised glacial valleys and uplands between the valleys showing limited erosion, indicating fast flowing ice in valleys and slowly moving ice on upland areas (cf. Kleman and Stroeven, 1997; Hall and Glasser, 2003; Sugden *et al*., 2005; Stroeven *et al*., 2013). Further inward is a zone of intermediate glacial erosion, Zone III, that includes large areas of scoured terrain with many bedrock knobs and water-filled basins (Figure 2(G) in Fu *et al*., 2013a). Zone IV, a central area, is narrow and constrained to the central high ridge, showing little erosion and having non-glacial landforms (Figure 2(B)). Glacial erosion principally occurs under warm-based basal ice and is negligible under cold-based ice (Sugden, 1968; Boulton, 1972; Kleman, 1994). The pattern of glacial erosion on the Haizishan Plateau, recognized on the basis of specific geomorphological characteristics (Fu *et al*., 2013a), indicates a discernable gradation of basal thermal conditions for the former ice caps, with warm-based erosive ice primarily under the peripheral parts of the ice cap, and cold-based or slowly-moving ice under the central parts of the ice dome, preserving relict landforms. The zonal division is illustrated in Figure 2(B); some uncertainty remains due to an uneven distribution of glacial landforms. The four zones represent the general landscape modification over the course of several glacial cycles (Fu *et al*., 2013b). Three sets of sinuous marginal moraines (M1–M3) (Figure 2(B)) in zone III are evidence for a most recent modification of the plateau surface by the LGM ice cap, including deposition during late-glacial stages (Fu *et al*., 2013b).

To quantify the erosional efficiency of the LGM ice cap, we sampled glacially eroded bedrock, glacial erratics, and river sand samples for *in situ* ^{10}Be and ^{26}Al analysis. This work extends a previous study by Fu *et al*. (2013b) that focused on glacial chronologies; here we investigate exposure-burial-erosion histories of individual bedrock samples. We derive inherited nuclide concentrations and from these estimate glacial erosion depths during the last glacial period and beyond. The details of the erosional pattern provide spatial information about basal thermal regimes and ice dynamics, particularly of the LGM Haizishan ice cap.

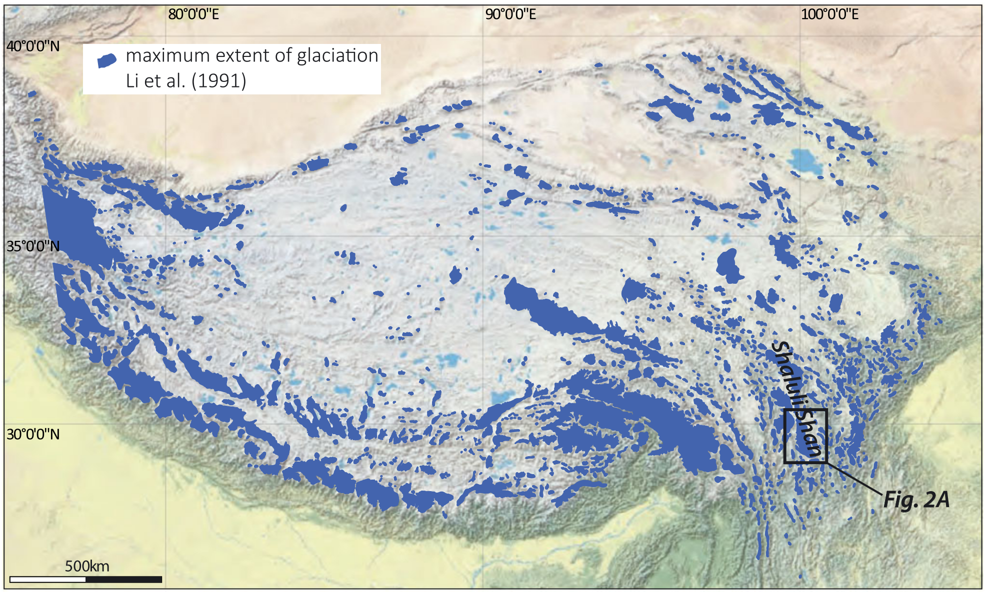

Figure 1. Tibetan Plateau showing the location of the study area (Figure 2(A)) and a reconstructed maximum extent of glaciation during the Quaternary period (Li *et al*., 1991). Base map is the world physical map from ArcGIS online services (http://services.arcgisonline.com/ArcGIS/rest/services). [Colour figure can be viewed at wileyonlinelibrary.com]

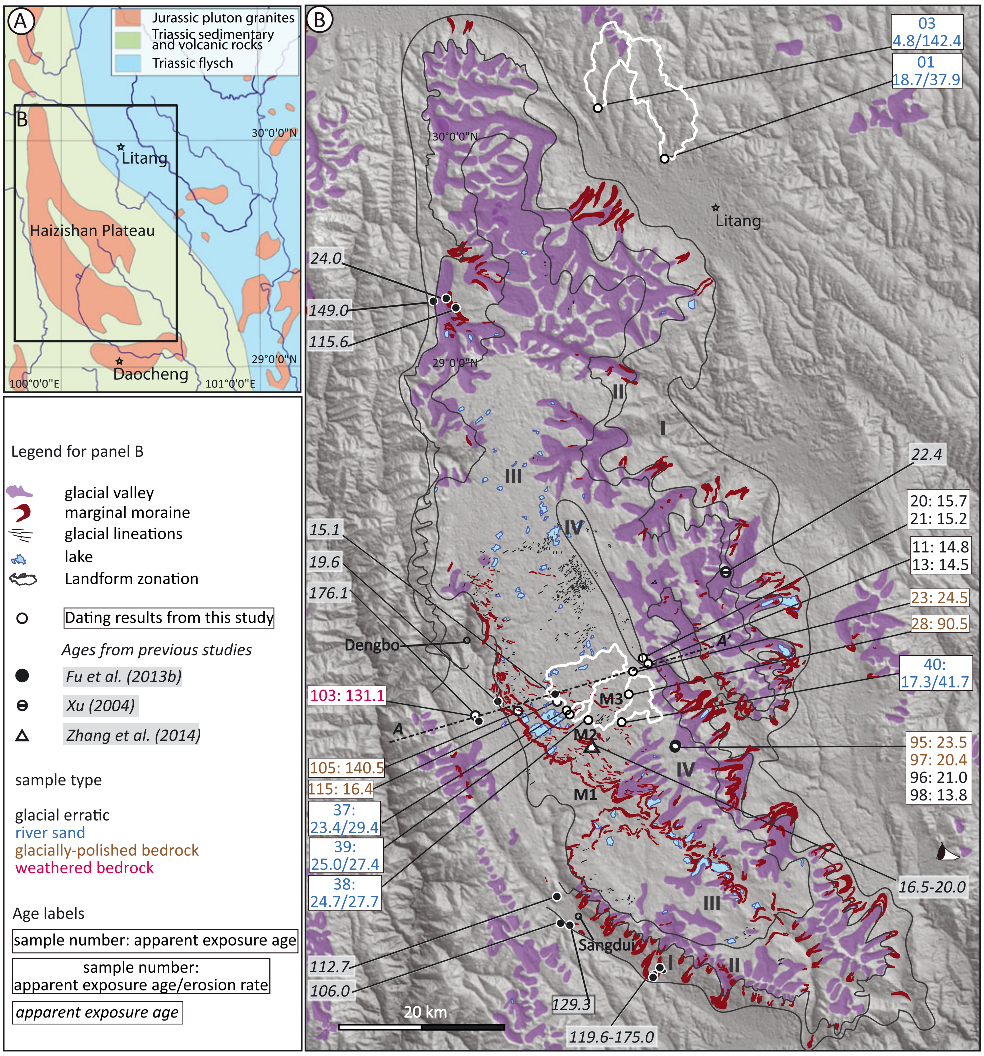

Figure 2. Glacial landforms of the study area (modified from Fu *et al.*, 2012), sample locations, and ^{10}Be apparent exposure ages (ka). (A) Simplified geological map of the Haizishan Plateau and its surrounding area (adapted from Ouimet *et al.*, 2010); (B) the Haizishan Plateau. M1-M3 denote three sinuous moraine stages. Age results are provided by sample number. Sampled river basins are delineated with white polygons. For river sand samples, average basin erosion rates (mm/ka) are listed. I–IV denotes erosion regions inferred from geomorphology (modified from Fu *et al.*, 2013a), where IV is the ice cap central region with little or no glacial erosion, III a wide zone of intermediate erosion, II a zone of strong erosion, and I a zone of deposition. A–A′ denotes a transect portrayed in Figures 5 and 6. The eye symbol denotes the viewing direction of Figure 5. [Colour figure can be viewed at wileyonlinelibrary.com]

Study area

Regional setting

The Haizishan Plateau is a low relief surface at 4000–5000 m above sea level (a.s.l.) in the Shaluli Shan, southeastern Tibetan Plateau, which is dominated by north–south trending mountains dissected by deeply incised rivers (Figures 1, 2(A)). Low-relief uplands are situated between the mountain ranges. Clark *et al.* (2005) interpreted these as relict landscapes formed at a lower elevation, then uplifted during the late Cenozoic (9–13 Ma) orogenesis of the eastern Tibetan Plateau. Among the relict landscapes on the southeastern margin of the Tibetan Plateau, the Haizishan Plateau is distinct, measuring 130 km north–south by 70 km east–west. It is separated from adjacent mountains by basins and valleys with floors below 4000 m a.s.l. A Jurassic granite pluton intruding into Triassic flysch (Ouimet *et al.*, 2010) forms the geology of the plateau (Figure 2(A)). Close to the central area of the Haizishan Plateau, an elongated north–south trending ridge of metamorphosed sedimentary rock rises ~300 m above the surrounding granite plateau surface. The plateau surface to the west of the ridge consists of a broad flat area, whereas high-relief terrain dominates to its east (Fu *et al.*, 2013a). The Haizishan region, currently (1981–2010), has a mean annual precipitation of 654 mm, a mean annual temperature of 4.8°C at 3728 m a.s.l., and a lapse rate of 5.2°C/km estimated from the two closest weather stations (CSMD, 2012). Its climate is strongly influenced by the southwest Asia summer monsoon system (Benn and Owen, 1998) that accounts for 86% of the annual precipitation in four months from June to September.

Glacial history

The Shaluli Shan has experienced several glaciations during the Quaternary, indicated by results from studies of glacial geomorphology and chronology of the Haizishan Plateau (Li *et al.*, 1986, 1991, 1996; Zheng and Ma, 1995; Zheng, 2001, 2006; Xu, 2004; Wang *et al.*, 2006; Xu and Zhou, 2009; Fu *et al.*, 2012, 2013a, b; Zhang *et al.*, 2014, 2015) and the surrounding mountains (Schäfer *et al.*, 2002; Owen *et al.*, 2005; Graf *et al.*, 2008; Strasky *et al.*, 2009; Xu *et al.*, 2010; Chevalier *et al.*, 2016). Using cosmogenic exposure ages from glacial erratics and in till profiles from the Shaluli Shan, Fu *et al.* (2013b) reconstructed the glacial chronology on and around the Haizishan Plateau. They found that glaciation occurred during the local Late Glacial, LGM, and in pre-LGM time. For exposure age consistency with new data, the published ages from Fu *et al.* (2013b) and from other references are recalculated with the expage-201806 calculator (expage.github.io/calculator) using the nuclide-specific LSD production rate scaling by Lifton *et al.* (2014). New exposure age results presented in this study are calculated using the same methodology (Supplementary Table 1).

Prior to the LGM, extensive ice caps covered the entire Haizishan Plateau (possibly several times) and extended into bordering mountains to the north and east; glaciers protruded into outlet valleys. A smaller ice cap existed during the LGM with outlet glaciers that terminated at the valley mouths, a few kilometers inside pre-LGM extents. The timing of this event comes from the oldest age (of three) for a latero-frontal moraine on the northern margin of the Haizishan Plateau of 24.0±1.6 ka (Fu *et al.*, 2013a, b). Three sets of prominent sinuous recessional moraines (M1–M3) were mapped across the western Haizishan Plateau; the outermost M1 and innermost M3 are dated to 19.6±1.3 ka and 15.1±1.1 ka (Late Glacial; ages calculated with zero erosion), respectively (oldest age from four boulders from M1 and oldest age of two boulders from M3; Figures 2B). During this time, ice caps on the plateau surface were separated from small ice fields or valley glaciers located on adjacent mountains to the west and north. The Haizishan Plateau is ice free today, although higher mountain ranges surrounding the plateau have glaciers commensurate with an equilibrium line altitude of 5600 m a.s.l. (Zheng, 2006).

Methods

To study the erosional efficiency of Haizishan ice caps, we measured cosmogenic nuclides (^{10}Be and ^{26}Al) from seven bedrock surfaces, and six erratics from various parts of the Haizishan Plateau. We also measured ^{10}Be concentrations from six river sand samples to investigate basin-wide erosion.

Sampling

Seventeen samples from the Haizishan Plateau were collected from different topographic settings in Zone III, including scoured terrain and bedrock outcrops in mountain passes (Figure 2(B)). Samples were chiseled from the top surfaces of glacial erratics and bedrock surfaces (Table I). Topographic shielding was based on measurements of strike and dip at breaks in slopes using a compass and clinometer. Elevation and coordinates were recorded with a handheld GPS.

We made an effort to sample glacial erratics and bedrock surfaces in close proximity to each other (cf. Fabel *et al.*, 2002; Stroeven *et al.*, 2011). The measurements of this study were supplemented by recalculated ages from erratics in Fu *et al.* (2013b).

Six river sand samples were collected at the outlets of six small catchments (Figure 2(B)). Four of these basins are located in Zone III on the Haizishan Plateau and were completely buried under ice during the last glaciation. For comparison, two river sand samples were collected from two catchments in nearby mountains to the north of the plateau (Figure 2(B)). These two basins have higher relief than those on the plateau surface, and only a small portion of one of the catchments has mapped glacial valleys (Fu *et al.*, 2012).

Laboratory methods and exposure age calculations

All samples were prepared for cosmogenic nuclide analysis at Purdue Rare Isotope Measurement Laboratory (PRIME Lab), following procedures by Kohl and Nishiizumi (1992). Isotope ratios were measured by accelerator mass spectrometry (AMS) at PRIME Lab. We measured ^{10}Be/^{9}Be and ^{26}Al/^{27}Al ratios using the 07KNSTD ^{10}Be standard (Nishiizumi *et al.*, 2007) and the KNSTD ^{26}Al standard (Nishiizumi, 2004). Process blanks of ^{10}Be/^{9}Be and ^{26}Al/^{27}Al ratios averaged $1.37 \pm 0.57 \times 10^{-14}$ (n = 2) and $2.59 \pm 6.03 \times 10^{-15}$ (n = 2), respectively. The blank corrections were insignificant for all samples. For Al measurements, we determined the total mass Al in the samples by ICP-OES from the aliquots prepared immediately after the samples had been dissolved. The total Al mass ranges from 2.380 to 4.412 mg in samples weighing from 8.506 to 35.229 g.

We calculated ^{10}Be and ^{26}Al apparent exposure ages using the expage-201806 calculator (http://expage.github.io/calculator) which is based on the CRONUS calculator (Balco *et al.*, 2008) but uses nuclide-specific LSD production rate scaling (Lifton *et al.*, 2014). The calculator uses reference spallation production rates of 3.98 ± 0.25 atoms/g/yr for ^{10}Be and 28.42 ± 1.87 atoms/g/yr for ^{26}Al, based on a global compilation of production rate calibration sites with well-clustered data (http://expage.github.io/production). The ^{10}Be half-life is 1.387×10^{6} yr (Chmeleff *et al.*, 2010; Korschinek *et al.*, 2010) and ^{26}Al half-life is 7.05×10^{5} yr (Nishiizumi, 2004). Apparent exposure ages were calculated assuming zero erosion and a rock density of 2.7 g/cm^3.

Glacial erosion

For bedrock samples with inherited nuclide concentrations resulting from prior exposure, glacial erosion can be quantified given a known exposure history of the sample (Stroeven *et al.*, 2002b; Fabel *et al.*, 2004; Goehring *et al.*, 2011; Li and Harbor, 2011; Young *et al.*, 2016). A simple approach to determine whether a sample has nuclide inheritance is comparing the apparent exposure age of the sample with an independent deglacial age of that sample location. An exposure age that is larger than the independent deglaciation age must be explained by prior exposure. The inherited component can be used to model the glacial erosion rate/amount. Critical assumptions in the model include the ice cover history and the interglacial erosion rate. In this study, we quantify the glacial erosion using the expage-201806 glacial erosion calculator (http://expage.github.io/calculator; glacialE.m). This involves the expage production rate calculations for spallation and muons, and ice cover histories determined by the Lisiecki and Raymo (2005) δ^{18}O record used as a proxy for global ice volume. For a given scenario, the calculator interpolates the glacial erosion rate that yields the input ^{10}Be and/or ^{26}Al concentration based on the output from a range of simulated glacial erosion rates (Figure 3).

We calculate glacial erosion for a range of scenarios, including total duration of nuclide production of 1 Ma and 120 ka, interglacial erosion rates of 0 and 2 mm/ka, and three ice cover histories defined by δ^{18}O cut-off values of 4.2‰, 4.5‰, and 4.8‰. The last deglaciation is set for each sample independently based on boulder ^{10}Be exposure ages (Supplementary Tables 2 and 3).

Basin-wide erosion

Cosmogenic nuclides in fluvial sediments can be used to determine long-term basin-wide erosion rates (Granger *et al.*, 1996;

Table I. Apparent exposure ages of samples from the Haizishan Plateau, southeastern Tibetan Plateau

Sample No.	Sample type; size of boulder (m); lithology	Latitude (N)	Longitude (E)	Elevation (m a.s.l.)	Shielding factor	depth (cm)[a]	^{10}Be conc. (atoms/g)[b]	^{10}Be error (atoms/g)	^{26}Al conc. (atoms/g)[b]	^{26}Al error (atoms/g)	$^{26}Al/^{10}Be$	^{10}Be age (ka)[c]	^{26}Al age (ka)[c]
Outlet valley head													
TB-09-95	bedrock; n.a.; granite with glacial polish	29.36888	100.23720	4692	1	3	1484567	56343	11184183	685313	7.5 ± 0.5	23.5 ± 1.6	26.1 ± 2.4
TB-09-97	bedrock; n.a.; granite with glacial polish	29.37080	100.23843	4676	1	4	1226343	41300	9560849	564865	7.8 ± 0.5	20.4 ±1.3	22.0 ± 1.9
TB-09-96	glacial erratic; 2*1*1.5; granite	29.36877	100.23717	4696	1	3	1306988	24057	9208488	506673	7.0 ± 0.4	21.0 ± 1.2	23.1 ± 2.1
TB-09-98	glacial erratic; 2*1*1.3; granite	29.37080	100.23843	4676	1	3	787410	36682				13.8 ± 1.0	
Scoured terrain in the middle section													
TB-09-103	bedrock; n.a.; weathered granite	29.40332	99.98970	4513	1	3.5	8605774	145572	58106136	4652360	6.8 ± 0.6	131.1 ± 7.8	136.4 ± 15.1
TB-09-105	bedrock; n.a.; granite with glacial polish	29.40835	100.04247	4486	1	5	8918399	189870	60173019	3348440	6.8 ± 0.4	140.5 ± 8.6	147.4 ± 13.7
TB-09-115	bedrock; n.a.; granite with glacial polish	29.41868	100.09108	4451	1	3	854821	50032	6094306	397647	7.2 ± 0.6	16.4 ± 1.3	17.5 ± 1.6
TB-11-23	bedrock; n.a.; granite with glacial polish	29.45046	100.18385	4712	1	3	1578238	33485				24.5 ± 1.5	
TB-11-28	bedrock; n.a.; granite with glacial polish	29.42608	100.17905	4664	1	3	6189190	144847	43428480	1178751	7.0 ± 0.3	90.6± 5.6	96.3 ± 7.2
TB-11-11	glacial erratic; 6*5*2; granite	29.45900	100.20301	4665	1	3	852073	16808				14.8 ± 0.9	
TB-11-13	glacial erratic; 1*1*0.5; granite	29.45900	100.20301	4665	1	3	832566	13699				14.5 ± 0.8	
TB-11-20	glacial erratic; 1.5*1*0.6; granite	29.46493	100.19632	4682	1	3	917037	23922				15.7 ± 1.0	
TB-11-21	glacial erratic; 0.5*0.5*0.5; granite	29.46473	100.19634	4670	1	3	880293	18390				15.2 ± 0.9	
Scoured terrain; small river basins													
TB-11-37	river sand; n.a.; n.a.;	29.40867	100.10253	4389	1		1273034	40412				23.4 ± 1.5	
TB-11-38	river sand; n.a.; n.a.;	29.39820	100.12917	4425	1		1379734	41876				24.7 ± 1.6	
TB-11-39	river sand; n.a.; n.a.;	29.40444	100.10627	4408	1		1384078	33631				25.0 ± 1.5	
TB-11-40	river sand; n.a.; n.a.;	29.39604	100.17000	4492	1		922177	26019				17.3 ± 1.1	
Nearby mountain area; small river basins													
TB-11-01	river sand; n.a.; n.a.;	30.00219	100.22415	3975	1		783196	23079				18.7 ± 1.2	
TB-11-03	river sand; n.a.; n.a.;	30.05683	100.14192	4038	1		199490	10833				4.8 ± 0.4	

[a]For glacial erratic and bedrock samples, sample depths equal the thickness of sampled rock.
[b]All ^{10}Be AMS results are standardized to 07KNSTD (Nishiizumi *et al.*, 2007), ^{26}Al AMS results are standardized to KNSTD (Nishiizumi, 2004) and assume no post-glacial shielding (bedrock erosion or vegetation- or snow covers).
[c]Exposure ages are derived from the time-varying production model of LSD (Lifton *et al.*, 2014).

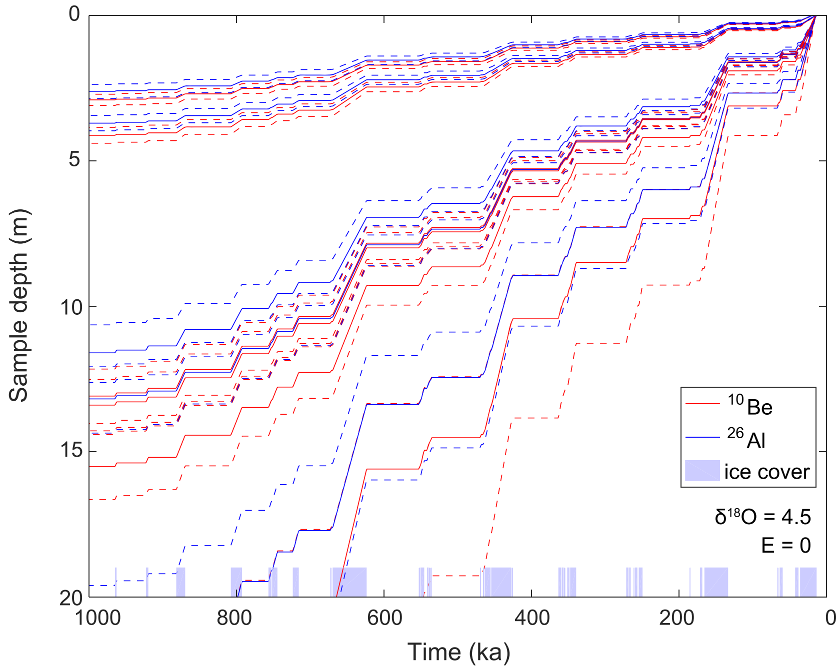

Figure 3. Erosion depth simulations of scenario 3 (Sim-3; Supplementary Table 2) for bedrock samples TB-09-95, TB-09-97, TB-09-105, TB-09-115, TB-11-23, and TB-11-28. [Colour figure can be viewed at wileyonlinelibrary.com]

von Blanckenburg, 2005; Granger and Riebe, 2014). The four samples from the plateau and two from the nearby mountain range enable a comparison of erosion in predominantly glacially and fluvially-modified landscapes, respectively. While a glacial landscape characterized by varying erosion rates over time violates the assumption of constant erosion rate (Granger *et al.*, 1996), the method still enables a first-order comparison of erosion rates, and of prior exposure of the Haizishan Plateau.

River sand samples were sieved to a grain size of 256–512 μm and were then processed in the same way as bedrock and boulder samples. Basin-wide erosion rates were calculated using the expage-201806 erosion rate calculator based on the erosion rate methodology from the CRONUS calculator (Balco *et al.*, 2008) but using the nuclide-specific LSD production rate scaling (Lifton *et al.*, 2014) for spallation and muons. For each catchment we used average coordinates, average atmospheric pressure based on the ERA40 interpolation (Lifton *et al.*, 2014) from the SRTM elevation with 90 m resolution (Jarvis *et al.*, 2008), and average topographic shielding factors based on Codilean (2006) and Li (2013).

Sample description

To study the erosional efficiency of the LGM ice cap, we sampled across the plateau surface at various distances from the inferred ice divide, Zone IV (Figure 2(B)). Sample TB-09-103 (Figures 4(A), 5) was collected from a deeply weathered granite bedrock ridge located 4 km outside the outermost sinuous moraine M1. It is located on the eastern slope of the mountain range along the western margin of the plateau. Between it and M1, a shallow depression extends several kilometers and parallels M1 and then joins rivers flowing northward and southward at its northern and southern ends, respectively. We

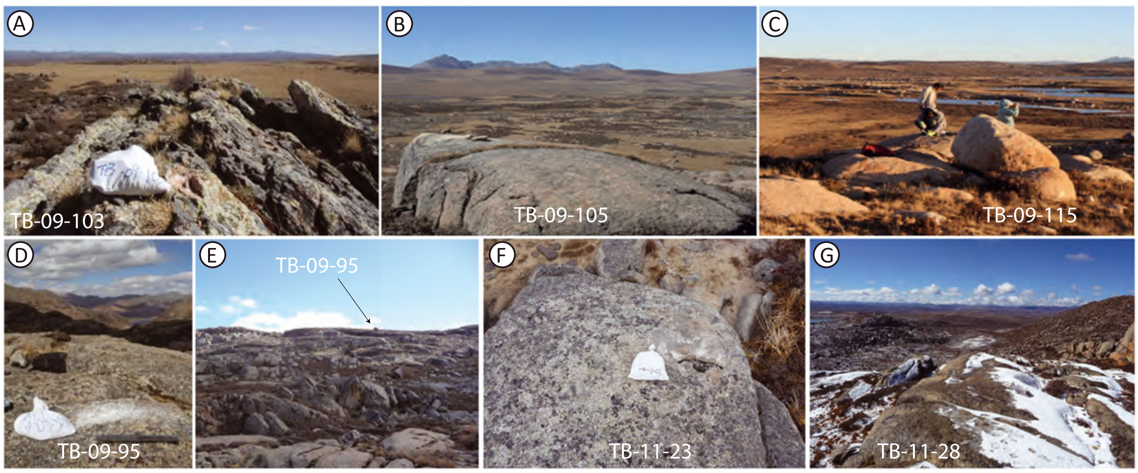

Figure 4. Photos of the bedrock sampled at TB-09-103 (A), TB-09-105 (B), TB-09-115 (C), TB-09-95 (D and E), TB-11-23 (F), and TB-11-28 (G). Panel E shows the glacially plucked rock steps at the head of the outlet valley where samples TB-09-95, 96, 97 and 98 are located (near the horizon denoted by the black arrow). [Colour figure can be viewed at wileyonlinelibrary.com]

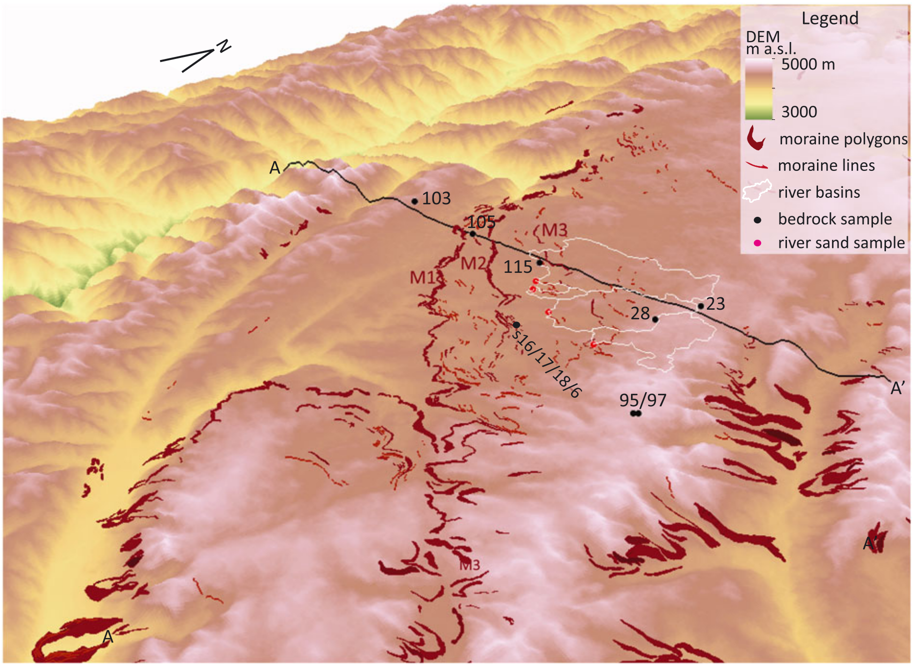

Figure 5. 3D view of the study area, including bedrock sample locations on the Haizishan Plateau analysed for erosion depths. The four river sand samples are denoted as red points. The location of transect A–A′ is given in Figure 2. [Colour figure can be viewed at wileyonlinelibrary.com]

collected two glacially-polished granite bedrock samples from inside moraine M1 (TB-09-105; Figures 4(B), 5), and outside the sinuous moraine M3 (TB-09-115; Figures 4(C), 5). Granite bedrock samples TB-09-95 (Figures 4(D), 4(E), 5) and TB-09-97 and erratic samples TB-09-96 and TB-09-98 were collected from the head of an outlet valley on the east side of the plateau. Abundant plucked and abraded landforms were observed at the head of the outlet valley, as expected for locations where ice converges into outlet valleys or fjords (Stroeven *et al.*, 2002a; Briner *et al.*, 2008; Figure 4(E)). Within 2 km NNW of this valley head along the eastern margin of the Haizishan Plateau, we sampled granite boulder samples TB-11-11, TB-11-13, TB-11-20, and TB-11-21 (Figure 2(B)). About 2 and 4 km southwest of these samples, we sampled granite bedrock samples TB-11-23 (Figures 4(F), 5) and TB-11-28 (Figures 4(G), 5), respectively, which are glacially polished surfaces. TB-11-23 was from bedrock located on a ridge and TB-11-28 from a roche moutonnée on a rock step. The sketch of the LGM ice cap profiles along the elevation transect AA′ on the plateau surface (Figure 6(A)) shows higher relief on the eastern slope than the western slope, corresponding to a shorter distance to the ice limits on the eastern slope than the western slope. According to the mapped moraines and lineations, the central dome of the LGM ice caps were likely residing on the central upland above 4600 m a.s.l. TB-11-23 and 28, and TB-09-95 and 97 were all collected from the eastern edge of the upland.

Four river sand samples were collected from scoured terrain on the Haizishan Plateau (TB-11-37, TB-11-38, TB-11-39, and TB-11-40). Another two river sand samples were collected from a mountain with limited evidence of glaciation immediately northwest of Litang (Figure 2(B)) (TB-11-01 and TB-11-03). The six catchments are relatively small (3–59 km^2) with gentle relief, reducing the likelihood of complicating factors such as landslides and long sediment residence times. The lithology

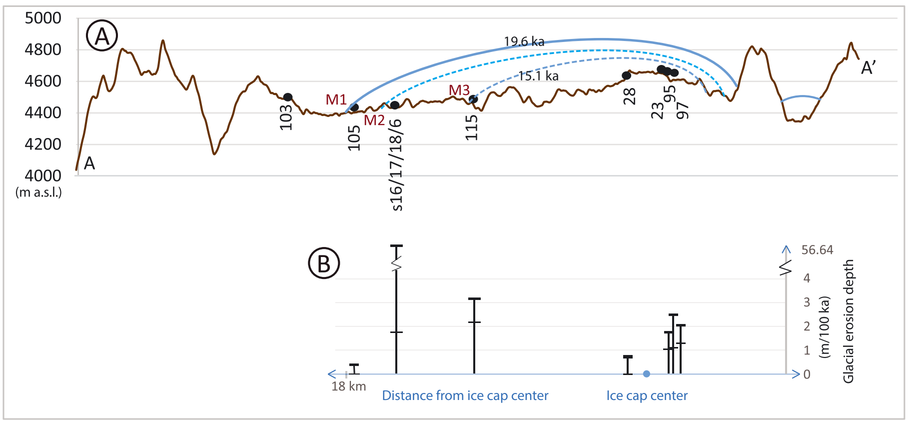

Figure 6. (A) Transect A–A′ (Figures 2, 5) and sample locations. Samples 28, 95, 97, s6/16/17/18 are projected to transect A–A′ based on their location relative to moraines M1–M3. The blue lines are schematic ice cap surface profiles. Glacier extents in the surrounding mountains are not indicated. (B) Plot of erosion depths of bedrock samples against the distance of each sample from the LGM ice cap center. The ice cap center was located between samples TB-11-23 and TB-11-28 as indicated by ice flow directions reconstructed from lineation and valley extending directions. The bold black lines indicate the modeled maximum erosion depth of the 12 scenarios and the thin line the minimum erosion depth (Table III; Supplementary Table 2). The results of the modeling for samples s6, s16, s17, and s18 are combined by taking the maximum and minimum from the 12 scenarios for all the four locations (Supplementary Table 2). [Colour figure can be viewed at wileyonlinelibrary.com]

of the plateau surface catchments is granite of the Jurassic pluton and catchments draining the adjacent mountain are set in Triassic volcanic and sedimentary rocks (Figure 2(A); Ouimet *et al.*, 2010).

All samples except TB-09-103 are located within the extents of the Late-Glacial ice cap delineated by M1 (Figures 2(B), 5, 6(A)). Based on the glacial history by Fu *et al.* (2013a, b) we reconstruct the maximum western expansion of the ice cap to have been between M1 and TB-09-103. So the nuclide inventories of all the samples except for TB-09-103 are assumed to result from similar exposure-burial histories until the LGM, but have experienced varying amounts of subglacial erosion. Individual deglaciation ages are applied.

Results and Interpretation

The apparent cosmogenic nuclide exposure ages are listed in Table I; six bedrock samples and one erratic sample have ^{26}Al exposure ages in addition to ^{10}Be ages. Estimates of glacial erosion rates from bedrock samples for ^{10}Be (^{26}Al) range from 0 to 307 (0–265) mm/ka and corresponding total erosion depths over the last 100 ka from 0 to 3.16 (0–2.73) m under different scenarios (Figure 6(B); Table II; Supplementary Table 2). Table III displays the ^{10}Be concentrations for the six river sand samples and calculated erosion rates and corresponding apparent exposure ages. Basin-wide erosion rates range from 27.4 to 142.4 mm/ka.

Glacial erosion from Haizishan Plateau bedrock samples

To estimate glacial erosion for the Haizishan Plateau bedrock samples within the LGM moraine, we use new and recalculated boulder ^{10}Be exposure ages (Fu *et al.*, 2013b; Table I; Supplementary Table 1) to determine the time of last deglaciation.

The two bedrock samples TB-09-105 and TB-09-115, located proximally to the two sinuous moraines dated to 19.6 ± 1.3 ka (M1) and 15.1 ± 1.1 ka (M3; Fu *et al.*, 2013b), were assigned deglaciation ages of 20 ka and 15 ka, respectively. For the two bedrock samples TB-11-23 and TB-11-28, the exposure ages of nearby boulder samples TB-11-11, TB-11-13, TB-11-20 and TB-11-21 (14.5 ± 0.8 to 15.7 ± 1.0 ka) and M3 (15.0 ± 1.0 and 15.1 ± 1.1 ka; Group K in supplementary Table 1; Fu *et al.*, 2013b) indicate deglaciation no earlier than 15 ka ago. For the valley head with two glacially-polished bedrock samples (TB-09-95 and TB-09-97), the two nearby erratic boulder samples yield exposure ages of 21.0 ± 1.2 ka (TB-09-96) and 13.8 ± 1.0 ka (TB-09-98; Figure 2(B)). Based on the youngest age of these two boulders, we use 14 ka as the valley head deglaciation age. This is slightly younger than the assigned deglaciation of M3 at 15 ka, but a later deglaciation of the valley head is supported by the presence of moraine segments mapped inside M3 (Figure 2(B)), and the fact that the valley head is 200-250 m higher than the plateau surface to the west.

The simulation scenarios with δ^{18}O cut-off values of 4.2 ‰, 4.5 ‰, and 4.8 ‰ yield total ice cover durations of 468 ka, 243 ka, and 55 ka over the last 1 Ma, and 59 ka, 29 ka, and 10 ka over the last 120 ka for the samples with deglaciation at 15 ka. Scenarios with shorter durations of ice cover yield larger depths of erosion (δ^{18}O: 4.8‰; 0–3.16 m over the last 100 ka based on ^{10}Be) than scenarios with longer durations of ice cover (δ^{18}O: 4.2‰; 0–2.59 m over the last 100 ka based on ^{10}Be). The assumption of an interglacial erosion rate of 2 mm/ka reduces the inferred depths of glacial erosion compared with scenarios with zero interglacial erosion, but the total depth of erosion is similar for both scenarios (Supplementary Figure 1; Supplementary Table 2).

The two granite bedrock samples from inside the sinuous moraines on the Haizishan Plateau yield apparent exposure ages of 140.5 ± 8.6 ka (TB-09-105) and 16.4 ± 1.3 ka (TB-09-115, Figure 2(B), Table I). The ~120 ka difference in apparent exposure age between M1 and the eroded bedrock surface just inside M1 implies that bedrock sample TB-09-105 has a large inherited nuclide inventory, which requires prior exposure before the last glacial cycle; it experienced little or no glacial erosion during the glaciation that deposited M1. The location of sample TB-09-105 close to the ice margin at maximum LGM expansion, implies that it would have been covered by thin ice with a high likelihood of being cold based and non-erosive. The apparent exposure age of TB-09-115 is slightly older than, but overlaps within uncertainties with, the age of moraine M3, indicating limited inheritance in sample TB-09-115. The concordance in age between the sinuous moraine M3 and the eroded bedrock surface just outside this moraine indicates that enough glacial erosion occurred during the last glaciation (2–3 m), thus removing the nuclide inventory from the last interglacial (Table III). These two bedrock samples are 5 km apart, are both from glacially-polished surfaces located on the crest of roche moutonnées (Figures 2, 4(B), 4(C)), but have apparently different erosion histories. The roche moutonnée of TB-09-105 was probably carved by a more extensive older glaciation, and that of TB-09-115 was at least modified during the LGM and Late Glacial events and was possibly entirely formed during these events. Distal to moraine M2, in-between moraines M1 and M3 at a location *c.* 7 km southeast of sample TB-09-115, there are four previously dated bedrock samples (s6/16/17/18) from a roche moutonnée (Zhang *et al.*, 2014, 2015). Recalculated ^{10}Be exposure ages of the bedrock samples range

Table II. Glacial erosion depth over the last 120 ka under different scenarios based ^{10}Be concentrations in bedrock samples. The bold and italic numbers are the minimum and maximum values of the 12 scenarios of each sample

Simulation No.		1	2	3	4	5	6	7	8	9	10	11	12
Simulation duration (Ma)		1	1	1	1	1	1	0.12	0.12	0.12	0.12	0.12	0.12
δ^{18}O		4.2	4.2	4.5	4.5	4.8	4.8	4.2	4.2	4.5	4.5	4.8	4.8
Interglacial erosion rate (mm/ka)		0	2	0	2	0	2	0	2	0	2	0	2
	TB-09-95	1.28	1.26	1.60	1.61	**1.77**	1.76	1.04	**1.03**	1.44	1.46	1.51	1.55
	TB-09-97	1.54	1.51	1.90	1.90	**2.03**	2.03	1.33	**1.31**	1.75	1.76	1.80	1.83
	TB-09-105	0.21	0.20	0.29	0.30	0.35	**0.38**	**0**	0.09	**0**	0.15	**0**	0.19
	TB-09-115	2.59	2.44	3.11	2.97	**3.16**	3.02	2.36	**2.23**	2.91	2.8	2.85	2.77
	TB-11-23	1.27	1.25	1.59	1.60	**1.74**	**1.74**	1.03	**1.02**	1.44	1.45	1.50	1.54
Glacial erosion depth over the last 100 ka (m)	TB-11-28	0.35	0.33	0.49	0.49	**0.68**	0.65	**0**	0.08	0.01	0.14	0.17	0.22

Table III. Apparent fluvial erosion rates calculated from river sand samples

	Average basin-wide latitude	Average basin-wide longitude	Average basin-wide atmospheric pressure (hPa)	Shielding factor	Erosion rate (mm/ka)[a]	Erosion rate error (mm/ka)	Apparent exposure age (ka)[b]	Basin slope (degree)	Basin slope error (degree)	Basin area (km^2)	Average erosion rates (mm/ka)
TB-11-37	29.446	100.123	4516.0	0.9970	29.4	2.0	22.7	7.6	4.6	37	
TB-11-38	29.422	100.155	4542.7	0.9970	27.7	1.9	24.0	7.9	4.5	23	
TB-11-39	29.409	100.121	4499.7	0.9980	27.4	1.8	24.3	7.9	4.2	3	
TB-11-40	29.420	100.191	4643.2	0.9970	41.7	2.8	16.0	9.3	5.9	16	31.5 ± 5.9
TB-11-01	30.069	100.219	4311.3	0.9870	37.9	2.6	17.5	14.4	7.1	27	
TB-11-03	30.109	100.152	4442.6	0.9880	142.4	11.6	4.7	14.6	7.8	59	90.2 ± 52.2

[a]Erosion rates are calculated using erosion.m from the expage-201806 calculator (expage.github.io/calculator) using the time-varying production model LSD (Lifton *et al.*, 2014).
[b]Apparent exposure ages are calculated assuming one period of continuous exposure at the surface and no erosion.

from 16.5 ± 1.2 ka to 20.0 ± 1.5 ka (Figure 2(B); Supplementary Table 1). These ages indicate that glacial erosion has removed some or most of the inherited cosmogenic nuclides similar to site TB-09-115.

Samples TB-11-23 and TB-11-28 are both located close to the heads of shallow valleys with TB-11-23 cut by ice flowing eastward and TB-11-28 cut by ice flowing westward. The apparent bedrock exposure ages for TB-11-23 (24.5 ± 1.5 ka) and TB-11-28 (90.6 ± 5.6 ka) imply nuclide inheritance. For the 1 Ma (120 ka) simulation scenarios, TB-11-23 yields a total depth of erosion of 1.25–1.74 m (1.02–1.54 m) and TB-11-28 yields a total depth of erosion of 0.33–0.68 m (0–0.22 m) over the last 100 ka.

TB-09-95 and TB-09-97 both have inheritance, and the calculated erosion depths over the last 100 ka at the head of the outlet valley are in the 1–2 m range (Table III). This is consistent with the presence of rock steps with steep plucked sides and smooth abraded stoss surfaces (Figure 4(E)).

Multiple nuclides: $^{26}Al/^{10}Be$ ratios and ^{26}Al ages

All seven ^{26}Al exposure ages from bedrock and erratic samples are generally consistent with corresponding ^{10}Be ages within uncertainties (Table I). Four of the seven samples have $^{26}Al/^{10}Be$ ratios which overlap within one sigma of the simple exposure line in the $^{26}Al/^{10}Be$ plot (Figure 7), and, if ^{26}Al and ^{10}Be production rate uncertainties are taken into account, all seven samples overlap within one sigma with the simple exposure line. The relatively high $^{26}Al/^{10}Be$ ratios might indicate that the samples have not experienced extensive periods of burial under non-erosive ice. However, there remains uncertainty, given the long half-lives of ^{10}Be and ^{26}Al, and the multiple ways that the $^{26}Al/^{10}Be$ ratios can be affected (Knudsen and Egholm, 2018).

River sediments samples

The four river sand samples from the formerly glaciated basins on the Haizishan Plateau yield ^{10}Be erosion rates ranging from 27.4 ± 1.8 mm/ka to 41.7 ± 2.8 mm/ka (Table III). The two mountain catchments with limited glacial evidence north of the Haizishan Plateau have ^{10}Be erosion rates of 37.9 ± 2.6 mm/ka and 142.4 ± 11.6 mm/ka. These erosion rates are calculated under the assumption that the surfaces have been eroded for a sufficiently long duration to achieve steady state ^{10}Be concentrations. If calculating apparent exposure ages from the ^{10}Be and average basin production rates and topographic shielding, and assuming continuous exposure of the sand at the surface, the Haizishan Plateau samples yield exposure ages ranging from 16.0 ka to 24.3 ka (Table III).

Exposure ages from boulders and bedrock in this study indicate a final deglaciation age of ~15 ka for the four river catchments on the Haizishan Plateau. The apparent exposure ages of the river sediments, assuming one period of full exposure at the surface, predate 22.7 ka (Table III) for three of four Haizishan basins (16.0 ka for one basin). This shows that glacial erosion did not pervasively remove the pre-glaciation nuclide inventory from the surface and near-surface rock and sediment.

Discussion

The rate of glacial erosion varied with location under the Haizishan ice cap. Widespread erosive landform features, such as outlet valleys, plucked bedrock basins, and roche

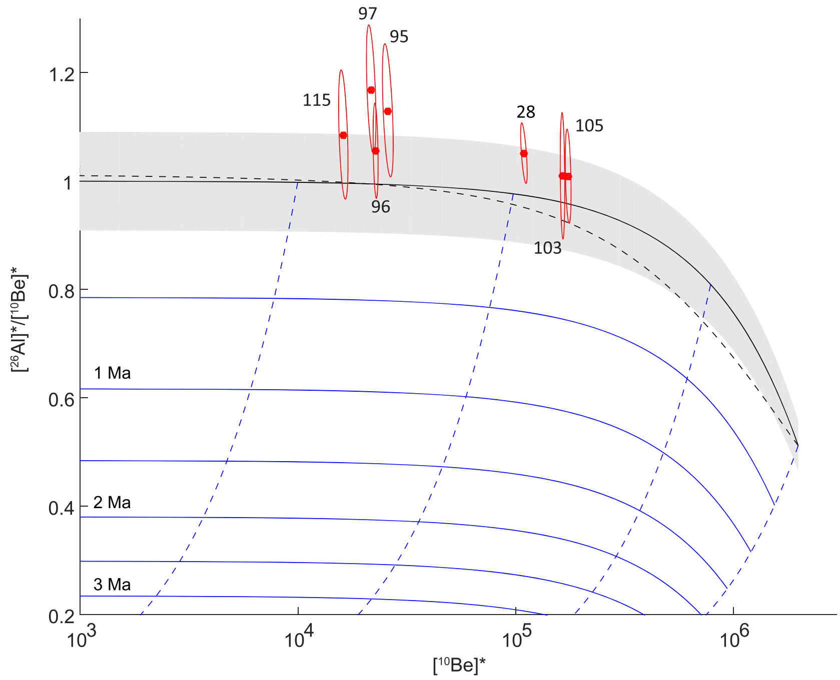

Figure 7. Plot of $^{26}Al/^{10}Be$ ratios against ^{10}Be concentrations, with the ^{26}Al and ^{10}Be concentrations individually normalized to long-term average sample ^{26}Al and ^{10}Be production rate from spallation and muon interaction. The numbers are the last two or three digits of the sample names. The black line shows the simple exposure line, and the grey area shows the uncertainty of the $^{26}Al/^{10}Be$ ratio assuming independent ^{26}Al and ^{10}Be production rate uncertainties. The dashed black line shows the end-point line for steady erosion. The blue sub-horizontal lines show the $^{26}Al/^{10}Be$ ratios for simple exposure followed by 0.5 Ma to 3 Ma of burial assuming full shielding from cosmic rays. The dashed blue sub-vertical lines show the $^{26}Al/^{10}Be$ ratio pathways for burial after 10 ka, 100 ka, 1 Ma and 10 Ma of surface exposure. [Colour figure can be viewed at wileyonlinelibrary.com]

moutonnées, indicate that there were areas of warm based ice under the Haizishan ice caps. This is consistent with some erosion estimates for bedrock samples in this study. The apparent exposure age of bedrock sample TB-09-115, at 16.4 ± 1.3 ka, almost overlaps with the deglaciation at ~15 ka. The modeled erosion yields a total of 2.23–3.16 m over the last 100 ka. Similarly, four bedrock samples close to M2 (samples s6, s16, s17, s18), dated by Zhang *et al.* (2014), yielded exposure ages of 16.5–20.0 ka, consistent with deglaciation ages and therefore considerable erosion of 1.71–56.64 m/ka.

Glacial lineation clusters and extensive sinuous moraines (totaling up to 50 km in length) on the Haizishan Plateau also indicate bedrock erosion, sediment transport and deposition by warm-based ice during LGM and Late Glacial time. At the same time, the Haizishan ice cap expanded into deep U-shaped outlet valleys towards the north and east of the plateau; thereby scouring the surface as ice flow converged and formed outlet glaciers. Some roches moutonnées in these outlet valleys have exposure ages similar to LGM (Figure 2(B); Xu, 2004; Supplementary Table 1) and indicate that enough erosion occurred during the last glaciation to reset the cosmogenic nuclide clock. Because production of cosmogenic nuclides occurs primarily in the uppermost few meters of rock, our data can only constrain a minimum estimate of subglacial erosion of a few meters. Further, it is likely that the erosion required to form roche moutonnées, stepped rock surfaces, and, especially, U-shaped valleys demands their formation during multiple glaciations (Harbor, 1992, 1995; Stroeven *et al.*, 2002a; Li *et al.*, 2005; Brook *et al.*, 2008).

Intermediate scales of glacial erosion are found at the edge of the central upland. For example, 1 to 2 m of erosion at an outlet valley head, as indicated by bedrock samples TB-09-95 and TB-09-97 (Figure 2(B); Table II), occurred in a transition zone from slow flowing ice on the plateau surface to fast flowing ice in an outlet valley. Landforms that reflect this change in subglacial dynamics include a transition from low-relief terrain on the plateau surface through rock steps at the outlet valley head formed by glacial plucking to deeply eroded U-shaped valleys (Stroeven *et al.*, 2002a). Similar erosion depths of 1–2 m per 100 ka were also modeled for sample TB-11-23. Although in a similar topographic setting to sample TB-11-23, location TB-11-28 has seen a lower modeled glacial erosion depth of 0–0.68 m per 100 ka. The tendency for higher amounts/rates of erosion along the eastern edge of the central upland, relative to its western edge, probably is a result of the reconstructed steeper slope of the ice surface in the east producing faster ice flow (Figure 5).

Cosmogenic inheritance in bedrock samples provides evidence for limited glacial erosion (0–0.38 m per 100 ka). Bedrock sample TB-09-105, which is just inside the Late Glacial margin of the ice cap (just up-ice of M1) and likely within 1 km of the LGM ice margin (Figures 2(B), 6(A)), has a large inherited cosmogenic isotope inventory indicating little or no erosion during the LGM. Glacial erosional features like roche moutonnées underneath some sinuous moraines in this area indicate that some of the glacial features were formed during pre-LGM and were preserved and then draped with sediment during LGM and Late Glacial times, which provides further evidence of a non-erosive marginal zone in this area.

While the overall landform pattern indicated in Figure 2(B) implies a concentric basal thermal regime pattern imprinted by extensive pre-LGM ice caps (Zheng and Ma, 1995; Kleman *et al.*, 2008; Fu *et al.*, 2013a), the occurrence of contrasting patterns of erosion and deposition over small distances in the scoured terrain (Figure 6(B)), probably reflects a patchiness in the basal thermal regime on smaller scales, as is evident for the Haizishan ice cap during the LGM and Late Glacial and also commonly inferred for Northern Hemisphere ice sheets (Kleman *et al.*, 1999; Kleman and Glasser, 2007; Stroeven *et al.*, 2013). The sinuous moraine ridges of M1 and the high nuclide inheritance in bedrock sample TB-09-105 indicate the non-erosive ice cap marginal depositional zone, followed by the strong erosion zone where TB-09-115 was collected. Four samples (s6, s16, s17, s18) from polished bedrock surfaces dated by Zhang *et al.* (2014) have similar apparent exposure ages to moraine M1 or are younger (Figure 2(B); Supplementary Table 1), indicating almost complete resetting of the nuclide clocks at these locations during LGM and Late Glacial. When modeled, s16 and s17 yield total glacial erosion depths ranging from 1.71 to 3.07 m, while s18 and s6 show a range from 3.29 to 56.64 m, for the last 100 ka (Supplementary Table 2). These results further support that a zone of strong erosion existed inside the non-erosive marginal zone underneath the LGM ice cap. The remaining four bedrock samples (TB-11-23, 28, 95, 97) collected from close to the center of the former ice cap, probably in positions close to underneath the ice divide, represent intermediate erosion of 0–2.03 m in the last 100 ka. Evidence for strong spatial gradients in the basal thermal regime furthermore comes from the distribution of lineations; large clusters of lineations are mapped close to the central relict ridge (IV in Figure 2(B)) and along M1, with few lineations on the flat scoured terrain in-between, indicating preservation underneath non-erosive ice below the former margin and ice-divide.

While bedrock ages at a range of locations on the plateau surfaces show that glacial erosion varied spatially during the LGM and the late glacial, basin-wide fluvial erosion rates provide insights into the average impact of glacial erosion across plateau catchments. The 22.7–24.3 ka apparent exposure ages (Table III) indicate that significant parts of the analysed basins experienced restricted (less than 1–3 m) glacial erosion. Previous studies show that glacial erosion tends to expose fresh bedrock surfaces which, upon postglacial weathering and erosion, tends to dilute nuclide concentrations in river sand, leading to an overestimation of fluvial erosion rates (Seong *et al.*, 2009b; Godard *et al.*, 2012). In contrast, this does not appear to be the case for our catchments on the Haizishan Plateau. Comparing our Haizishan Plateau basins with data from nearby mountain areas (Ouimet *et al.*, 2010), the Haizishan Plateau basin erosion rates are significantly lower than most of the erosion rates from non-glaciated fluvial basins. Since our basins have gentler slopes than the majority of basins sampled by Ouimet *et al.* (2010), these results provide qualitative support for the notion that fluvial erosion rates scale with basin slope. With an average erosion rate of 31.5 ± 5.9 mm/ka (Table III), the Haizishan Plateau has low fluvial erosion rates, even in comparison with other locations on the Tibetan Plateau (Li *et al.*, 2014, and reference therein). This indicates that, despite significantly higher fluvial erosion rates consuming the margin of the Tibetan Plateau (Stroeven *et al.*, 2009; Li *et al.*, 2014; Ansberque *et al.*, 2015), low-relief relict surfaces at the Tibetan Plateau margins, such as the Haizishan Plateau, tend to be the most stable landscape elements.

Several lines of evidence indicate that the basal thermal regime of the former Haizishan ice caps exhibited a zonal pattern. It is likely that the zonal pattern of landforms (Zheng and Ma, 1995; Fu *et al.*, 2013a) reflects the integrated effect of glacial erosion and deposition over multiple glaciations. The smaller LGM – Late Glacial Haizishan ice cap deposited moraines that drape older glacial lineations and glacially polished bedrock. The discrepancy in flow directions between various lineation clusters also indicates that ice flow patterns and basal thermal zones changed between glaciations or in different stages of a glaciation. Such changes are also implicated in emerging ice cap modeling results (Fu, 2013), which include the migration of ice divides during the growth and decay of ice caps on the Haizishan Plateau. Because the basal thermal regime of the LGM Haizishan ice cap helped shape and modify the observed landform zonation pattern, topography played an important role in observed differences in amounts of erosion between the eastern and western margin of the central upland. Subglacial thermal boundaries were likely not uniform but irregular and patchy, particularly where boundaries between erosional zones are inferred. Such boundaries are probably interweaved, as indicated by pronounced differences in erosion over relatively short distances.

Conclusions

We use ^{10}Be and ^{26}Al cosmogenic nuclide apparent exposure ages from bedrock, glacial erratics, and river sand to examine the erosion pattern of former Haizishan ice caps on the southeastern Tibetan Plateau. Both the pattern of glacial landforms and the ^{10}Be and ^{26}Al data indicate that the ice caps that advanced and retreated across a high-elevation plateau surface, typically had a concentric basal thermal regime but with strong spatial gradients during the last glacial period. For example, the ice cap plucked rock steps at the heads of outlet valleys and exerted intermediate erosion (0–2 m) where the ice surface slope was steep and ice flow converged into a valley. Intermediate depths of glacial erosion across much of the Haizishan Plateau is consistent with a nuclide inheritance detected in the cosmogenic inventory of sand samples from rivers draining scoured terrain. A patchy subglacial thermal regime is evident from the close proximity of locations with high erosion rates and limited erosion rates, such as underneath and immediately inside the LGM margin on the Haizishan Plateau. In particular, roche moutonnées formed during a previous glaciation are draped by end moraines, strongly indicating preservation during the last glaciation, and a central relict ridge is juxtaposed with lineations. These all attest that the glacial landscape reflects the integrated impact of multiple glaciations with pronounced spatial patterns of erosion and preservation.

Erosion patterns determined using cosmogenic nuclide dating techniques not only support the conclusions of prior studies that used geomorphological mapping to suggest a zonal pattern of thermal regimes, but also provide insights into glacial landscape development as a time-transgressive process driven by the evolution of former ice caps. Our study is the first to show clear evidence of preservation under ice on the Tibetan Plateau. Future work using glacial modeling to investigate the basal thermal conditions of the former Haizishan ice cap may yield further insights in the underlying mechanisms that drive the development of glacial erosion patterns.

Acknowledgements—We thank Jin Yao and Zhang Mei for field assistance and Johan Kleman for discussions. We thank Jane Lund Andersen and two anonymous reviewers for constructive comments and criticism. Funding for fieldwork and cosmogenic dating was provided by the National Natural Science Foundation of China grant to Fu (41501067), and the Swedish Research Council/Swedish International Development Cooperation Agency (VR/SIDA) - Swedish Research link grants to Stroeven (578 348-2004-5684 and 348-2007-6924), and through Swedish Society for Anthropology and Geography, Royal Swedish Academy of Sciences, and Carl Mannerfelts scholarships to Fu. Harbor's effort was supported in part by a Marie Curie International Incoming Fellowship within the 7th European Community Framework Program. Caffee and PRIME Lab acknowledge support from NSF (EAR-1153689).

References

Amundson JM, Iverson NR. 2006. Testing a glacial erosion rule using hang heights of hanging valleys, Jasper National Park, Alberta, Canada. *Journal of Geophysical Research* **111**: F01020. https://doi.org/10.1029/2005jf000359.

Andrews JT, LeMasurier WE. 1973. Rates of Quaternary glacial erosion and corrie formation, Marie Byrd Land, Antarctica. *Geology* **1**: 75–80. https://doi.org/10.1130/0091-7613(1973)1<75:roqgea>2.0.co;2.

Ansberque C, Godard V, Bellier O, De Sigoyer J, Liu-Zeng J, Xu X, Ren Z, Li Y, Team ASTER. 2015. Denudation pattern across the Longriba fault system and implications for the geomorphological evolution of the eastern Tibetan margin. *Geomorphology* **246**: 542–557. https://doi.org/10.1016/j.geomorph.2015.07.017.

Balco G. 2011. Contributions and unrealized potential contributions of cosmogenic-nuclide exposure dating to glacier chronology, 1990–2010. *Quaternary Science Reviews* **30**: 3–27. https://doi.org/10.1016/j.quascirev.2010.11.003.

Balco G, Stone JO, Lifton NA, Dunai TJ. 2008. A complete and easily accessible means of calculating surface exposure ages or erosion rates from 10Be and 26Al measurements. *Quaternary Geochronology* **3**: 174–195. https://doi.org/10.1016/j.quageo.2007.12.001.

Benn DI, Owen LA. 1998. The role of the Indian summer monsoon and the mid-latitude westerlies in Himalayan glaciation: review and speculative discussion. *Journal of the Geological Society* **155**: 353–363. https://doi.org/10.1144/gsjgs.155.2.0353.

Bierman PR, Marsella KA, Patterson C, Davis PT, Caffee M. 1999. Mid-Pleistocene cosmogenic minimum-age limits for pre-Wisconsinan glacial surfaces in southwestern Minnesota and southern Baffin Island: a multiple nuclide approach. *Geomorphology* **27**: 25–39. https://doi.org/10.1016/S0169-555X(98)00088-9.

Boulton GS. 1972. Modern Arctic glaciers as depositional models for former ice sheets. *Journal of the Geological Society* **128**: 361–393. https://doi.org/10.1144/gsjgs.128.4.0361.

Braun J, Zwartz D, Tomkin JH. 1999. A new surface-processes model combining glacial and fluvial erosion. *Annals of Glaciology* **28**: 282–290. https://doi.org/10.3189/172756499781821797.

Briner JP, Lifton NA, Miller GH, Refsnider K, Anderson R, Finkel R. 2014. Using *in situ* cosmogenic 10Be, 14C, and 26Al to decipher the history of polythermal ice sheets on Baffin Island, Arctic Canada. *Quaternary Geochronology* **19**: 4–13. https://doi.org/10.1016/j.quageo.2012.11.005.

Briner JP, Miller GH, Davis PT, Bierman PR, Caffee M. 2003. Last Glacial Maximum ice sheet dynamics in Arctic Canada inferred from young erratics perched on ancient tors. *Quaternary Science Reviews* **22**: 437–444. https://doi.org/10.1016/S0277-3791(03)00003-9.

Briner JP, Miller GH, Finkel R, Hess DP. 2008. Glacial erosion at the fjord onset zone and implications for the organization of ice flow on Baffin Island, Arctic Canada. *Geomorphology* **97**: 126–134. https://doi.org/10.1016/j.geomorph.2007.02.039.

Briner JP, Swanson TW. 1998. Using inherited cosmogenic 36Cl to constrain glacial erosion rates of the Cordilleran ice sheet. *Geology* **26**: 3–6. https://doi.org/10.1130/0091-7613(1998)026<0003:uicctc>2.3.co;2.

Brocklehurst SH. 2010. Tectonics and geomorphology. *Progress in Physical Geography* **34**: 357–383. https://doi.org/10.1177/0309133309360632.

Brocklehurst SH, Whipple KX. 2006. Assessing the relative efficiency of fluvial and glacial erosion through simulation of fluvial landscapes. *Geomorphology* **75**: 283–299. https://doi.org/10.1016/j.geomorph.2005.07.028.

Brook MS, Kirkbride MP, Brock BW. 2006. Quantified time scale for glacial valley cross-profile evolution in alpine mountains. *Geology* **34**: 637–640. https://doi.org/10.1130/G22700.1.

Brook MS, Kirkbride MP, Brock BW. 2008. Temporal constraints on glacial valley cross-profile evolution: Two Thumb Range, central Southern Alps, New Zealand. *Geomorphology* **97**: 24–34. https://doi.org/10.1016/j.geomorph.2007.02.036.

Chevalier M-L, Leloup PH, Replumaz A, Pan J, Liu D, Li H, Gourbet L, Métois M. 2016. Tectonic-geomorphology of the Litang fault system, SE Tibetan Plateau, and implication for regional seismic hazard. *Tectonophysics* **682**: 278–292. https://doi.org/10.1016/j.tecto.2016.05.039.

Chmeleff J, von Blanckenburg F, Kossert K, Jakob D. 2010. Determination of the Be-10 half-life by multicollector ICP-MS and liquid scintillation counting. *Nuclear Instruments and Methods in Physics Research Section B-Beam Interactions with Materials and Atoms* **268**: 192–199. https://doi.org/10.1016/j.nimb.2009.09.012.

Clark MK, House MA, Royden LH, Whipple KX, Burchfiel BC, Zhang X, Tang W. 2005. Late Cenozoic uplift of southeastern Tibet. *Geology* **33**: 525–528. https://doi.org/10.1130/G21265.1.

Codilean AT. 2006. Calculation of the cosmogenic nuclide production topographic shielding scaling factor for large areas using DEMs. *Earth Surface Processes and Landforms* **31**: 785–794. https://doi.org/10.1002/esp.1336.

Colgan PM, Bierman PR, Mickelson DM, Caffee M. 2002. Variation in glacial erosion near the southern margin of the Laurentide Ice Sheet, south-central Wisconsin, USA: Implications for cosmogenic dating of glacial terrains. *GSA Bulletin* **114**: 1581–1591. https://doi.org/10.1130/0016-7606(2002)114<1581:VIGENT>2.0.CO;2.

Cowan EA, Seramur KC, Powell RD, Willems BA, Gulick SPS, Jaeger JM. 2010. Fjords as temporary sediment traps: history of glacial erosion and deposition in Muir Inlet, Glacier Bay National Park, southeastern Alaska. *Geological Society of America Bulletin* **122**: 1067–1080. https://doi.org/10.1130/b26595.1.

CSMD (China surface monthly meteorological data collection (1981–2010)), 2012. China Meteorological Information Center, http://data.cma.cn/data/detail/dataCode/A.0029.0004.html.

Cui ZJ. 1981a. Cirques at the head of Urumqi River, Tian Shan. *Journal of Glaciology and Geocryology* **3**: 24–25 (in Chinese, English abstract).

Cui ZJ. 1981b. Glacial erosion landforms and development of trough at the head of Urumqi River, Tian Shan. *Journal of Glaciology and Geocryology* **3**: 1–15 (in Chinese, English abstract).

Davis PT, Bierman PR, Marsella KA, Caffee MW, Southon JR. 1999. Cosmogenic analysis of glacial terrains in the eastern Canadian Arctic: a test for inherited nuclides and the effectiveness of glacial erosion. *Annals of Glaciology* **28**: 181–188.

Delmas M, Calvet M, Gunnell Y. 2009. Variability of Quaternary glacial erosion rates – a global perspective with special reference to the Eastern Pyrenees. *Quaternary Science Reviews* **28**: 484–498. https://doi.org/10.1016/j.quascirev.2008.11.006.

Dowdeswell JA, Ottesen D, Rise L. 2010. Rates of sediment delivery from the Fennoscandian Ice Sheet through an ice age. *Geology* **38**: 3–6. https://doi.org/10.1130/g25523.1.

Egholm DL, Jansen JD, Brædstrup CF, Pedersen VK, Andersen JL, Ugelvig SV, Larsen NK, Knudsen MF. 2017. Formation of plateau landscapes on glaciated continental margins. *Nature Geoscience* **10**: 592–597. https://doi.org/10.1038/ngeo2980.

Egholm DL, Pedersen VK, Knudsen MF, Larsen NK. 2012. Coupling the flow of ice, water, and sediment in a glacial landscape evolution model. *Geomorphology* **141–142**: 47–66. https://doi.org/10.1016/j.geomorph.2011.12.019.

Fabel D, Harbor J. 1999. The use of in-situ produced cosmogenic radionuclides in glaciology and glacial geomorphology. *Annals of Glaciology* **28**: 103–110. https://doi.org/10.3189/172756499781821968.

Fabel D, Harbor J, Dahms D, James A, Elmore D, Horn L, Daley K, Steele C. 2004. Spatial patterns of glacial erosion at a valley scale derived from terrestrial cosmogenic 10Be and 26Al concentrations in rock. *Annals of the Association of American Geographers* **94**: 241–255.

Fabel D, Stroeven AP, Harbor J, Kleman J, Elmore D, Fink D. 2002. Landscape preservation under Fennoscandian ice sheets determined from *in situ* produced 10Be and 26Al. *Earth and Planetary Science Letters* **201**: 397–406.

Fu P. 2013. Paleoglaciology of Shaluli Shan, southeastern Tibetan Plateau. PhD thesis, Stockholm University, Stockholm.

Fu P, Harbor JM, Stroeven AP, Hättestrand C, Heyman J, Zhou L. 2013a. Glacial geomorphology and paleoglaciation patterns in Shaluli Shan, the southeastern Tibetan Plateau – evidence for polythermal ice cap glaciation. *Geomorphology* **182**: 66–78. https://doi.org/10.1016/j.geomorph.2012.10.030.

Fu P, Heyman J, Hättestrand C, Stroeven AP, Harbor JM. 2012. Glacial geomorphology of the Shaluli Shan area, southeastern Tibetan Plateau. *Journal of Maps* **8**: 48–55. https://doi.org/10.1080/17445647.2012.668762.

Fu P, Stroeven AP, Harbor JM, Hättestrand C, Heyman J, Caffee MW, Zhou L. 2013b. Paleoglaciation of Shaluli Shan, southeastern Tibetan Plateau. *Quaternary Science Reviews* **64**: 121–135. https://doi.org/10.1016/j.quascirev.2012.12.009.

Godard V, Burbank DW, Bourlès DL, Bookhagen B, Braucher R, Fisher GB. 2012. Impact of glacial erosion on 10Be concentrations in fluvial sediments of the Marsyandi catchment, central Nepal. *Journal of Geophysical Research: Earth Surface* **117**: F03013. https://doi.org/10.1029/2011JF002230.

Goehring BM, Schaefer JM, Schluechter C, Lifton NA, Finkel RC, Jull AJT, Akçar N, Alley RB. 2011. The Rhone Glacier was smaller than today for most of the Holocene. *Geology* **39**: 679–682. https://doi.org/10.1130/G32145.1.

Gosse JC, Phillips FM. 2001. Terrestrial *in situ* cosmogenic nuclides: theory and application. *Quaternary Science Reviews* **20**: 1475–1560. https://doi.org/10.1016/s0277-3791(00)00171-2.

Graf AA, Strasky S, Zhao ZZ, Akçar N, Ivy-Ochs S, Kubik PW, Christl M, Kasper HU, Wieler R, Schlüchter C. 2008. Glacier extension on the eastern Tibetan Plateau in response to MIS 2 cooling, with a contribution to 10Be and 21Ne methodology. In *Glacial Response to Global Climate Changes: Cosmogenic Nuclide Chronologies from High and Low Latitudes*, Strasky S (ed) . ETH Zürich; 77–110.PhD thesis

Granger DE, Riebe CS. 2014. Cosmogenic nuclides in weathering and erosion. In *Treatise on Geochemistry* (2nd edn), Holland HD, Turekian KK (eds). Elsevier: Oxford; 401–436. DOI: https://doi.org/10.1016/B978-0-08-095975-7.00514-3

Granger DE, Kirchner JW, Finkel R. 1996. Spatially averaged long-term erosion rates measured from *in situ*-produced cosmogenic nuclides in alluvial sediment. *The Journal of Geology* **104**: 249–257. https://doi.org/10.1086/629823.

Granger DE, Lifton NA, Willenbring JK. 2013. A cosmic trip: 25 years of cosmogenic nuclides in geology. *Geological Society of America Bulletin* **125**: 1379–1402. https://doi.org/10.1130/B30774.1.

Hall AM, Glasser NF. 2003. Reconstructing the basal thermal regime of an ice stream in a landscape of selective linear erosion: Glen Avon, Cairngorm Mountains, Scotland. *Boreas* **32**: 191–207. https://doi.org/10.1080/03009480310001100.

Hallet B, Hunter L, Bogen J. 1996. Rates of erosion and sediment evacuation by glaciers: a review of field data and their implications. *Global and Planetary Change* **12**: 213–235. https://doi.org/10.1016/0921-8181(95)00021-6.

Harbor J, Stroeven AP, Fabel D, Clarhäll A, Kleman J, Li Y, Elmore D, Fink D. 2006. Cosmogenic nuclide evidence for minimal erosion across two subglacial sliding boundaries of the late glacial Fennoscandian ice sheet. *Geomorphology* **75**: 90–99. https://doi.org/10.1016/j.geomorph.2004.09.036.

Harbor JM. 1992. Numerical modeling of the development of U-shaped valleys by glacial erosion. *Geological Society of America Bulletin* **104**: 1364–1375.

Harbor JM. 1995. Development of glacial-valley cross sections under conditions of spatially variable resistance to erosion. *Geomorphology* **14**: 99–107. https://doi.org/10.1016/0169-555X(95)00051-1.

Harbor JM, Hallet B, Raymond CF. 1988. A numerical-model of landform development by glacial erosion. *Nature* **333**: 347–349.

Herman F, Braun J. 2008. Evolution of the glacial landscape of the Southern Alps of New Zealand: insights from a glacial erosion model. *Journal of Geophysical Research-Earth Surface* **113**: F02009. https://doi.org/10.1029/2007jf000807.

Herman F, Braun J, Deal E, Prasicek G. 2018. The response time of glacial erosion. *Journal of Geophysical Research: Earth Surface* **123**: 801–817. https://doi.org/10.1002/2017JF004586.

Heyman J, Stroeven AP, Caffee MW, Hättestrand C, Harbor JM, Li Y, Alexanderson H, Zhou L, Hubbard A. 2011a. Palaeoglaciology of Bayan Har Shan, NE Tibetan Plateau: exposure ages reveal a missing LGM expansion. *Quaternary Science Reviews* **30**: 1988–2001. https://doi.org/10.1016/j.quascirev.2011.05.002.

Heyman J, Stroeven AP, Harbor JM, Caffee MW. 2011b. Too young or too old: evaluating cosmogenic exposure dating based on an analysis of compiled boulder exposure ages. *Earth and Planetary Science Letters* **302**: 71–80. https://doi.org/10.1016/j.epsl.2010.11.040.

Hooke RL, Elverhøi A. 1996. Sediment flux from a fjord during glacial periods, Isfjorden, Spitsbergen. *Global and Planetary Change* **12**: 237–249. https://doi.org/10.1016/0921-8181(95)00022-4.

Ivy-Ochs S, Akçar N, Timothy Jull AJ. 2014. Tracking the pace of quaternary landscape change with cosmogenic nuclides. *Quaternary Geochronology* **19**: 1–3. https://doi.org/10.1016/j.quageo.2013.10.001.

Jaeger JM, Koppes MN. 2016. The role of the cryosphere in source-to-sink systems. *Earth-Science Reviews* **153**: 43–76. https://doi.org/10.1016/j.earscirev.2015.09.011.

Jamieson SSR, Hulton NRJ, Hagdorn M. 2008. Modelling landscape evolution under ice sheets. *Geomorphology* **97**: 91–108. https://doi.org/10.1016/j.geomorph.2007.02.047.

Jamieson SSR, Sugden DE, Hulton NRJ. 2010. The evolution of the subglacial landscape of Antarctica. *Earth and Planetary Science Letters* **293**: 1–27. https://doi.org/10.1016/j.epsl.2010.02.012.

Jarvis A, Reuter HI, Nelson A, Guevara E. 2008. Hole-filled seamless SRTM data V4. International Centre for Tropical Agriculture (CIAT) [online] Available from: http://srtm.csi.cgiar.org

Kleman J. 1994. Preservation of landforms under ice sheets and ice caps. *Geomorphology* **9**: 19–32.

Kleman J, Hättestrand C, Clarhäll A. 1999. Zooming in on frozen-bed patches: scale-dependent controls on Fennoscandian ice sheet basal thermal zonation. *Annals of Glaciology*: 189–194.

Kleman J, Glasser N. 2007. The subglacial thermal organisation (STO) of ice sheets. *Quaternary Science Reviews* **26**: 585–597. https://doi.org/10.1016/j.quascirev.2006.12.010.

Kleman J, Stroeven AP. 1997. Preglacial surface remnants and quaternary glacial regimes in northwestern Sweden. *Geomorphology* **19**: 35–54.

Kleman J, Stroeven AP, Lundqvist J. 2008. Patterns of Quaternary ice sheet erosion and deposition in Fennoscandia and a theoretical framework for explanation. *Geomorphology* **97**: 73–90. https://doi.org/10.1016/j.geomorph.2007.02.049.

Knudsen MF, Egholm DL. 2018. Constraining quaternary ice covers and erosion rates using cosmogenic 26Al/10Be nuclide concentrations. *Quaternary Science Reviews* **181**: 65–75. https://doi.org/10.1016/j.quascirev.2017.12.012.

Knudsen MF, Egholm DL, Jacobsen BH, Larsen NK, Jansen JD, Andersen JL, Linge HC. 2015. A multi-nuclide approach to constrain landscape evolution and past erosion rates in previously glaciated terrains. *Quaternary Geochronology* **30**: 100–113. https://doi.org/10.1016/j.quageo.2015.08.004.

Kohl C, Nishiizumi K. 1992. Chemical isolation of quartz for measurement of *in situ*-produced cosmogenic nuclides. *Geochimica et Cosmochimica Acta* **56**: 3583–3587. https://doi.org/10.1016/0016-7037(92)90401-4.

Koppes M, Hallet B. 2006. Erosion rates during rapid deglaciation in Icy Bay, Alaska. *Journal of Geophysical Research* **111**: F02023. https://doi.org/10.1029/2005jf000349.

Koppes M, Hallet B, Rignot E, Mouginot J, Wellner JS, Boldt K. 2015. Observed latitudinal variations in erosion as a function of glacier dynamics. *Nature* **526**: 100–103. https://doi.org/10.1038/nature15385.

Koppes MN, Montgomery DR. 2009. The relative efficacy of fluvial and glacial erosion over modern to orogenic timescales. *Nature Geoscience* **2**: 644–647. https://doi.org/10.1038/ngeo616.

Korschinek G, Bergmaier G, Faestermann T, Knie K, Rugel G, Waller A, Dillmann I, Dollinger G, von Gostomski CL, Lpssert K, Maiti M, Poutivtsev M, Remmert A. 2010. A new value for the half-life of 10Be by Heavy-Ion Elastic Recoil Detection and liquid scintillation counting. *Nuclear Instruments and Methods in Physics Research Section B: Beam Interactions with Materials and Atoms* **268**: 187–191. https://doi.org/10.1016/j.nimb.2009.09.020.

Li BY, Li JJ, Cui ZJ, Zheng BX, Zhang QS, Wang FB, Zhou SZ, Shi ZH, Jiao KQ, Kang JC. 1991. *Quaternary glacial distribution map of Qinghai-Xizang (Tibet) plateau*. Science Press: Beijing Mapscale 1:3 000 000 (in Chinese).

Li JJ, Feng Z, Zhou SZ. 1996. The Quaternary glacial remnants in Hengduan Shan. In *Glaciers in Hengduan Shan*, Li JJ, Su Z (eds). Science Press: Beijing; 157–212 (in Chinese).

Li JJ, Yao TD, Feng ZD. 1986. The evolution pattern of the Daocheng Paleo ice cap. In *Collections of Expedition to the Hengduan Mountain*, Vol. **2**. Beijing Science and Technology Publishing House: Beijing; 269–279.

Li Y, Li D, Liu G, Harbor J, Caffee M, Stroeven AP. 2014. Patterns of landscape evolution on the central and northern Tibetan Plateau investigated using *in situ* produced 10Be concentrations from river sediments. *Earth and Planetary Science Letters* **398**: 77–89. https://doi.org/10.1016/j.epsl.2014.04.045.

Li YK. 2013. Determining topographic shielding from digital elevation models for cosmogenic nuclide analysis: a GIS approach and field validation. *Journal of Mountain Science* **10**: 355–362. https://doi.org/10.1007/s11629-013-2564-1.

Li YK, Fabel D, Stroeven AP, Harbor J. 2008. Unraveling complex exposure-burial histories of bedrock surfaces under ice sheets by integrating cosmogenic nuclide concentrations with climate proxy records. *Geomorphology* **99**: 139–149. https://doi.org/10.1016/j.geomorph.2007.10.010.

Li YK, Harbor J, Stroeven AP, Fabel D, Kleman J, Fink D, Caffee M, Elmore D. 2005. Ice sheet erosion patterns in valley systems in northern Sweden investigated using cosmogenic nuclides. *Earth Surface Processes and Landforms* **30**: 1039–1049. https://doi.org/10.1002/esp.1261.

Li YK, Harbor JM. 2011. Cosmogenic nuclides and geomorphology: theory, limitations and applications. In *Geomorphology and Plate Tectonics*, Ferrari D, Guiseppi A (eds). NOVA; 1–33.

Li YK, Liu GN, Cui ZJ. 2001. Longitudinal variations in cross-section morphology along a glacial valley: a case-study from the Tien Shan, China. *Journal of Glaciology* **47**: 243–250. https://doi.org/10.3189/172756501781832278.

Lifton N, Sato T, Dunai TJ. 2014. Scaling *in situ* cosmogenic nuclide production rates using analytical approximations to atmospheric cosmic-ray fluxes. *Earth and Planetary Science Letters* **386**: 149–160. https://doi.org/10.1016/j.epsl.2013.10.052.

Lisiecki LE, Raymo ME. 2005. A Pliocene-Pleistocene stack of 57 globally distributed benthic δ18O records. *Paleoceanography* **20**: PA1003. https://doi.org/10.1029/2004PA001071.

MacGregor KR, Anderson RS, Anderson SP, Waddington ED. 2000. Numerical simulations of glacial-valley longitudinal profile evolution. *Geology* **28**: 1031–1034. https://doi.org/10.1130/0091-7613(2000)28<1031:nsoglp>2.0.co;2.

MacGregor KR, Anderson RS, Waddington ED. 2009. Numerical modeling of glacial erosion and headwall processes in alpine valleys. *Geomorphology* **103**: 189–204. https://doi.org/10.1016/j.geomorph.2008.04.022.

Marquette GC, Gray JT, Gosse JC, Courchesne F, Stockli L, Macpherson G, Finkel R. 2004. Felsenmeer persistence under non-erosive ice in the Torngat and Kaumajet mountains, Quebec and Labrador, as determined by soil weathering and cosmogenic nuclide exposure dating. *Canadian Journal of Earth Sciences* **41**: 19–38. https://doi.org/10.1139/e03-072.

Melanson A, Bell T, Tarasov L. 2013. Numerical modelling of subglacial erosion and sediment transport and its application to the North American ice sheets over the Last Glacial cycle. *Quaternary Science Reviews* **68**: 154–174. https://doi.org/10.1016/j.quascirev.2013.02.017.

Miller GH, Briner JP, Lifton NA, Finkel RC. 2006. Limited ice-sheet erosion and complex exposure histories derived from *in situ* cosmogenic 10Be, 26Al, and 14C on Baffin Island, Arctic Canada. *Quaternary Geochronology* **1**: 74–85. https://doi.org/10.1016/j.quageo.2006.06.011.

Montgomery DR. 2002. Valley formation by fluvial and glacial erosion. *Geology* **30**: 1047–1050.

Nesje A, Dahl SO, Valen V, Øvstedal J. 1992. Quaternary erosion in the Sognefjord drainage basin, western Norway. *Geomorphology* **5**: 511–520. https://doi.org/10.1016/0169-555X(92)90022-G.

Nishiizumi K. 2004. Preparation of 26Al AMS standards. *Nuclear Instruments and Methods in Physics Research Section B: Beam Interactions with Materials and Atoms* **223–224**: 388–392. https://doi.org/10.1016/j.nimb.2004.04.075.

Nishiizumi K, Imamura M, Caffee MW, Southon JR, Finkel RC, McAninch J. 2007. Absolute calibration of 10Be AMS standards. *Nuclear Instruments and Methods in Physics Research Section B: Beam Interactions with Materials and Atoms* **258**: 403–413. https://doi.org/10.1016/j.nimb.2007.01.297.

Ouimet W, Whipple K, Royden L, Reiners P, Hodges K, Pringle M. 2010. Regional incision of the eastern margin of the Tibetan Plateau. *Lithosphere* **2**: 50–63. https://doi.org/10.1130/l57.1.

Owen LA, Caffee MW, Bovard KR, Finkel RC, Sharma MC. 2006. Terrestrial cosmogenic nuclide surface exposure dating of the oldest glacial successions in the Himalayan orogen: Ladakh Range, northern India. *Geological Society of America Bulletin* **118**: 383–392. https://doi.org/10.1130/b25750.1.

Owen LA, Derbyshire E, Scott CH. 2003. Contemporary sediment production and transfer in high-altitude glaciers. *Sedimentary Geology* **155**: 13–36. https://doi.org/10.1016/S0037-0738(02)00156-2.

Owen LA, Finkel RC, Barnard PL, Haizhou M, Asahi K, Caffee MW, Derbyshire E. 2005. Climatic and topographic controls on the style and timing of Late Quaternary glaciation throughout Tibet and the Himalaya defined by 10Be cosmogenic radionuclide surface exposure dating. *Quaternary Science Reviews* **24**: 1391–1411. https://doi.org/10.1016/j.quascirev.2004.10.014.

Patton H, Hubbard A, Andreassen K, Auriac A, Whitehouse PL, Stroeven AP, Shackleton C, Winsborrow M, Heyman J, Hall AM. 2017. Deglaciation of the Eurasian ice sheet complex. *Quaternary Science Reviews* **169**: 148–172. https://doi.org/10.1016/j.quascirev.2017.05.019.

Phillips WM, Hall AM, Mottram R, Fifield LK, Sugden DE. 2006. Cosmogenic 10Be and 26Al exposure ages of tors and erratics, Cairngorm Mountains, Scotland: timescales for the development of a classic landscape of selective linear glacial erosion. *Geomorphology* **73**: 222–245. https://doi.org/10.1016/j.geomorph.2005.06.009.

Rahaman W, Singh SK, Sinha R, Tandon SK. 2009. Climate control on erosion distribution over the Himalaya during the past ~100 ka. *Geology* **37**: 559–562. https://doi.org/10.1130/G25425A.1.

Schäfer JM, Tschudi S, Zhao Z, Wu X, Ivy-Ochs S, Wieler R, Baur H, Kubik PW, Schlüchter C. 2002. The limited influence of glaciations in Tibet on global climate over the past 170 000 yr. *Earth and Planetary Science Letters* **194**: 287–297.

Seong YB, Owen LA, Caffee MW, Kamp U, Bishop MP, Bush A, Copland L, Shroder JF. 2009a. Rates of basin-wide rockwall retreat in the K2 region of the Central Karakoram defined by terrestrial cosmogenic nuclide Be-10. *Geomorphology* **107**: 254–262. https://doi.org/10.1016/j.geomorph.2008.12.014

Seong YB, Owen LA, Yi C, Finkel RC, Schoenbohm L. 2009b. Geomorphology of anomalously high glaciated mountains at the northwestern end of Tibet: Muztag Ata and Kongur Shan. *Geomorphology* **103**: 227–250. https://doi.org/10.1016/j.geomorph.2008.04.025.

Shi Y. 1992. Glaciers and glacial geomorphology in China. *Zeitschrift für Geomorphologie* **86**: 19–35.

Shi Y. 2002. Characteristics of late Quaternary monsoonal glaciation on the Tibetan Plateau and in East Asia. *Quaternary International* **97/98**: 79–91.

Staiger JKW, Gosse JC, Johnson JV, Fastook J, Gray JT, Stockli DF, Stockli L, Finkel R. 2005. Quaternary relief generation by polythermal glacier ice. *Earth Surface Processes and Landforms* **30**: 1145–1159. https://doi.org/10.1002/esp.1267.

Staiger JW, Gosse J, Little EC, Utting DJ, Finkel R, Johnson JV, Fastook J. 2006. Glacial erosion and sediment dispersion from detrital cosmogenic nuclide analyses of till. *Quaternary Geochronology* **1**: 29–42. https://doi.org/10.1016/j.quageo.2006.06.009.

Sternai P, Herman F, Valla PG, Champagnac J-D. 2013. Spatial and temporal variations of glacial erosion in the Rhône valley (Swiss Alps): insights from numerical modeling. *Earth and Planetary Science Letters* **368**: 119–131. https://doi.org/10.1016/j.epsl.2013.02.039.

Strasky S, Graf AA, Zhao Z, Kubik PW, Baur H, Schlüchter C, Wieler R. 2009. Late Glacial ice advances in southeast Tibet. *Journal of Asian Earth Sciences* **34**: 458–465. https://doi.org/10.1016/j.jseaes.2008.07.008.

Stroeven AP, Hättestrand C, Heyman J, Harbor J, Li YK, Zhou LP, Caffee MW, Alecanderson H, Ma HZ, Liu GN. 2009. Landscape analysis of the Huang He headwaters, NE Tibetan Plateau - patterns of glacial and fluvial erosion. *Geomorphology* **103**: 212–226. https://doi.org/10.1016/j.geomorph.2008.04.024.

Stroeven AP, Fabel D, Harbor J, Hättestrand C, Kleman J. 2002a. Quantifying the Erosional Impact of the Fennoscandian Ice Sheet in the Torneträsk-Narvik Corridor, Northern Sweden, Based on Cosmogenic Radionuclide Data. *Geografiska Annaler Series A, Physical Geography* **84**: 275–287. https://doi.org/10.2307/3566145.

Stroeven AP, Fabel D, Harbor JM, Fink D, Caffee MW, Dahlgren T. 2011. Importance of sampling across an assemblage of glacial landforms for interpreting cosmogenic ages of deglaciation. *Quaternary Research* **76**: 148–156. https://doi.org/10.1016/j.yqres.2011.04.004.

Stroeven AP, Fabel D, Hättestrand C, Harbor J. 2002b. A relict landscape in the centre of Fennoscandian glaciation: cosmogenic radionuclide evidence of tors preserved through multiple glacial cycles. *Geomorphology* **44**: 145–154. https://doi.org/10.1016/S0169-555X(01)00150-7.

Stroeven AP, Harbor J, Heyman J. 2013. Erosional landscapes. In *Treatise on Geomorphology*, Shroder JF (ed). Academic Press, San Diego, 100–112. DOI: https://doi.org/10.1016/B978-0-12-374739-6.00198-6

Sugden DE. 1968. The selectivity of glacial erosion in the Cairngorm Mountains, Scotland. *Transactions of the Institute of British Geographers* **45**: 79. https://doi.org/10.2307/621394.

Sugden DE. 1978. Glacial erosion by the Laurentide ice sheet. *Journal of Glaciology* **20**: 367–391.

Sugden DE, Balco G, Cowdery SG, Stone JO, Sass LC, III. 2005. Selective glacial erosion and weathering zones in the coastal mountains of Marie Byrd Land, Antarctica. *Geomorphology* **67**: 317–334. https://doi.org/10.1016/j.geomorph.2004.10.007.

Sugden DE, Hein AS, Woodward J, Marrero SM, Rodés Á, Dunning SA, Stuart FM, Freeman SPHT, Winter K, Westoby MJ. 2017. The million-year evolution of the glacial trimline in the southernmost Ellsworth Mountains, Antarctica. *Earth and Planetary Science Letters* **469**: 42–52. https://doi.org/10.1016/j.epsl.2017.04.006.

Swift DA, Persano C, Stuart FM, Gallagher K, Whitham A. 2008. A reassessment of the role of ice sheet glaciation in the long-term evolution of the East Greenland fjord region. *Geomorphology* **97**: 109–125. https://doi.org/10.1016/j.geomorph.2007.02.048.

Tomkin JH, Braun J. 2002. The influence of alpine glaciation on the relief of tectonically active mountain belts. *American Journal of Science* **302**: 169–190. https://doi.org/10.2475/ajs.302.3.169.

Torres MA, Moosdorf N, Hartmann J, Adkins JF, West AJ. 2017. Glacial weathering, sulfide oxidation, and global carbon cycle feedbacks. *Proceedings of the National Academy of Sciences* **114**: 8716–8721. https://doi.org/10.1073/pnas.1702953114.

Ugelvig SV, Egholm DL, Iverson NR. 2016. Glacial landscape evolution by subglacial quarrying: a multiscale computational approach. *Journal of Geophysical Research: Earth Surface* **121**: 2042–2068. https://doi.org/10.1002/2016JF003960.

van der Beek P, Bourbon P. 2008. A quantification of the glacial imprint on relief development in the French western Alps. *Geomorphology* **97**: 52–72. https://doi.org/10.1016/j.geomorph.2007.02.038.

von Blanckenburg F. 2005. The control mechanisms of erosion and weathering at basin scale from cosmogenic nuclides in river sediment. *Earth and Planetary Science Letters* **237**: 462–479. https://doi.org/10.1016/j.epsl.2005.06.030.

Wang J, Raisbeck G, Xu X, Yiou F, Bai S. 2006. *In situ* cosmogenic 10Be dating of the Quaternary glaciations in the southern Shaluli Mountain on the Southeastern Tibetan Plateau. *Science in China Series D: Earth Sciences* **49**: 1291–1298. https://doi.org/10.1007/s11430-006-2026-5.

Whipple KX. 2009. The influence of climate on the tectonic evolution of mountain belts. *Nature Geoscience* **2**: 97–104. https://doi.org/10.1038/ngeo413.

Xu L, Zhou S. 2009. Quaternary glaciations recorded by glacial and fluvial landforms in the Shaluli Mountains, Southeastern Tibetan Plateau. *Geomorphology* **103**: 268–275. https://doi.org/10.1016/j.geomorph.2008.04.015.

Xu LB, Ou XJ, Lai ZP, Zhou SZ, Wang J, Fu YC. 2010. Timing and style of Late Pleistocene glaciation in the Queer Shan, northern Hengduan Mountains in the eastern Tibetan Plateau. *Journal of Quaternary Science* **25**: 957–966. https://doi.org/10.1002/jqs.1379.

Xu X. 2004. Study on Quaternary Ice Age event of Mountain Shaluli in the Southeast of Qinghai-Xizang Plateau by cosmogenic isotope 10Be. PhD Thesis, Nanjing Normal University, Nanjing.

Yanites BJ, Ehlers TA. 2012. Global climate and tectonic controls on the denudation of glaciated mountains. *Earth and Planetary Science Letters* **325–326**: 63–75. https://doi.org/10.1016/j.epsl.2012.01.030.

Young NE, Briner JP, Maurer J, Schaefer JM. 2016. 10Be measurements in bedrock constrain erosion beneath the Greenland Ice Sheet margin. *Geophysical Research Letters* **43**: 2016GL070258. https://doi.org/10.1002/2016GL070258.

Zhang Z, Wang J, Xu X, Bai S, Chang Z. 2015. Cosmogenic 10Be and 26Al chronology of the Last Glaciation of the Palaeo-Daocheng Ice Cap, Southeastern Qinghai-Tibetan Plateau. *Acta Geologica Sinica - English Edition* **89**: 575–584. https://doi.org/10.1111/1755-6724.12448.

Zhang Z, Xu X, Wang J, Zhao Z, Bai S, Chang Z. 2014. Last Deglaciation Climatic Fluctuation Record by the Palaeo-Daocheng Ice Cap, Southeastern Qinghai-Tibetan Plateau. *Acta Geologica Sinica - English Edition* **88**: 1863–1874. https://doi.org/10.1111/1755-6724.12352.

Zheng BX. 2001. Study on the quaternary glaciation and the formation of the Moxi platform in the east slopes of the M ount Gongga. *Journal of Glaciology and Geocryology* **283–291**(in Chinese, English abstract): 23.

Zheng BX. 2006. Quaternary glaciations in the Hengduan Mountains. In *The Quaternary Glaciations and Environmental Variations in China*, Shi YF, Cui ZJ, Su Z (eds). Hebei Science and Technology Publishing House; 407–441 (in Chinese, English abstract).

Zheng BX, Ma QH. 1995. A study on the geomorphological characteristics and glaciations in Paleo-Daocheng Ice Cap, western Sichuan. *Journal of Glaciology and Geocryology* **17**: 23–32 (in Chinese).

Supporting Information

Additional supporting information may be found online in the Supporting Information section at the end of the article.

Supplementary Figure 1. Plots of the erosion depth simulations for 12 scenarios presented in Supplementary Table 2.
Supplementary Table 1. Results of recalculated ages of samples from previous studies using expage-201806 at http://expage.github.io/calculator
Supplementary Table 2. Glacial erosion rates and depths over the last 100 ka and 1 Ma for 12 different scenarios, based on ^{10}Be concentrations in bedrock samples. The simulation period is 1 Ma for all the simulations
Supplementary Table 3. Inputs for the glacial erosion calculation (expage.github.io/calculator) listed in Supplementary Table 2

